AD-A166 624 THE REBATRON AS A HIGH ENERGY ACCELERATOR(U) NAVAL RESEARCH LAB WASHINGTON DC D DIALETIS ET AL. 04 APR 86 NRL-MR-5655 1/1

UNCLASSIFIED F/G 20/7 NL

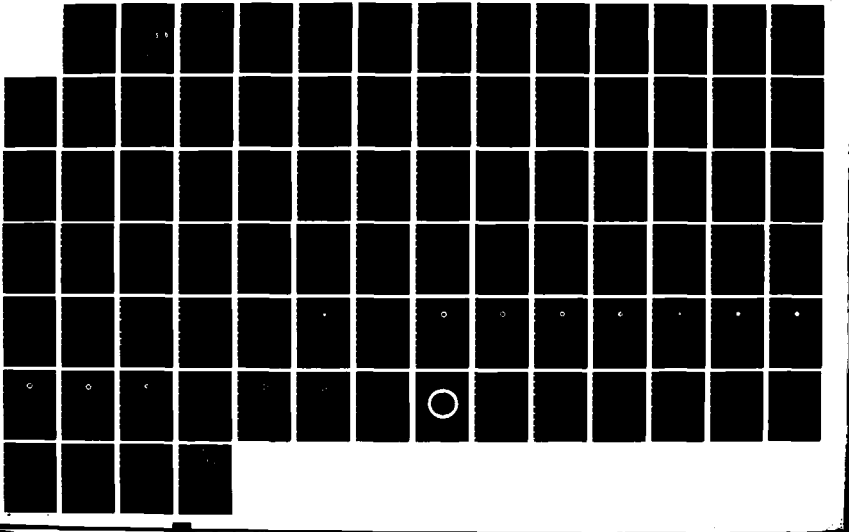

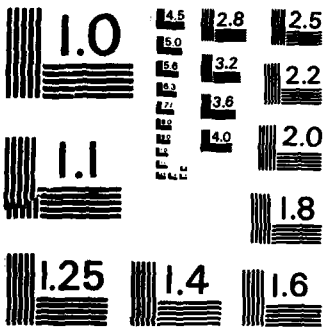

(2)

NRL Memorandum Report 5655

The REBATRON as a High Energy Accelerator

D. DIALETIS,* S. J. MARSH† AND C. A. KAPETANAKOS

Plasma Physics Division

**Science Applications International Corporation*
McLean, VA 22102

†Sachs/Freeman Associates
Landover, MD 20785

April 4, 1986

NAVAL RESEARCH LABORATORY
Washington, D.C.

SECURITY CLASSIFICATION OF THIS PAGE

AD-A166 624

REPORT DOCUMENTATION PAGE

1a. REPORT SECURITY CLASSIFICATION UNCLASSIFIED	1b. RESTRICTIVE MARKINGS
2a. SECURITY CLASSIFICATION AUTHORITY	3. DISTRIBUTION / AVAILABILITY OF REPORT Approved for public release; distribution unlimited.
2b. DECLASSIFICATION / DOWNGRADING SCHEDULE	
4. PERFORMING ORGANIZATION REPORT NUMBER(S) NRL Memorandum Report 5655	5. MONITORING ORGANIZATION REPORT NUMBER(S)
6a. NAME OF PERFORMING ORGANIZATION Naval Research Laboratory 6b. OFFICE SYMBOL (If applicable) Code 4710	7a. NAME OF MONITORING ORGANIZATION Office of Naval Research
6c. ADDRESS (City, State, and ZIP Code) Washington, DC 20375-5000	7b. ADDRESS (City, State, and ZIP Code) Arlington, VA 22217
8a. NAME OF FUNDING / SPONSORING ORGANIZATION ONR and BRL 8b. OFFICE SYMBOL (If applicable)	9. PROCUREMENT INSTRUMENT IDENTIFICATION NUMBER
8c. ADDRESS (City, State, and ZIP Code) Arlington, VA 22217 Aberdeen, MD	10. SOURCE OF FUNDING NUMBERS PROGRAM ELEMENT NO. 61153N; PROJECT NO.; TASK NO. RR011-09-4E; WORK UNIT ACCESSION NO. DN180-207

11. TITLE (Include Security Classification)
The REBATRON as a High Energy Accelerator

12. PERSONAL AUTHOR(S)
Dialetis, D.,* Marsh, S. J.,† and Kapetanakos, C. A.

13a. TYPE OF REPORT	13b. TIME COVERED	14. DATE OF REPORT (Year, Month, Day)	15. PAGE COUNT
Interim	FROM _____ TO _____	1986 April 4	86

16. SUPPLEMENTARY NOTATION *Science Applications International Corporation, McLean, VA 22102
†Sachs/Freeman Associates, Landover, MD 20785

17. COSATI CODES			18. SUBJECT TERMS (Continue on reverse if necessary and identify by block number)
FIELD	GROUP	SUB-GROUP	Accelerators, Induction accelerators, Electron beams

19. ABSTRACT (Continue on reverse if necessary and identify by block number)

A detailed numerical and analytical study of the beam dynamics in a rebatron acceleration has shown that energies approaching 1 GeV can be achieved within 5-10 microseconds. Since the acceleration in the rebatron occurs within a short time, the device may not be sensitive to the various instabilities and the loss to synchrotron radiation should be small. The rapid acceleration is produced by convoluted parallel transmission lines, which provide a high gradient electric field. At the initial stage of the acceleration, the beam is confined inside the torus by a strong focusing torsatron magnetic field, which makes the beam insensitive to the mismatch and to the external field index of a vertical magnetic field. This local field is generated by two coaxial cylindrical plates located symmetrically around the minor axis of the torus, and carrying currents in opposite directions. The energy of the beam increases in synchronism with the vertical magnetic field so that the beam remains matched (i.e., the beam radius remains constant) during the entire acceleration. As a result of the periodic nature of the acceleration, it was found that resonances can be excited, which cause the orbits to expand. The only disruptive resonance occurs at $\gamma \approx 1830$, i.e., when the vertical magnetic field reaches twice the value of the toroidal magnetic field. Keywords:

20. DISTRIBUTION / AVAILABILITY OF ABSTRACT	21. ABSTRACT SECURITY CLASSIFICATION
☒ UNCLASSIFIED/UNLIMITED ☐ SAME AS RPT ☐ DTIC USERS	UNCLASSIFIED
22a. NAME OF RESPONSIBLE INDIVIDUAL C. A. Kapetanakos	22b. TELEPHONE (Include Area Code) (202) 767-2838 22c. OFFICE SYMBOL Code 4710

DD FORM 1473, 84 MAR 83 APR edition may be used until exhausted
All other editions are obsolete

SECURITY CLASSIFICATION OF THIS PAGE

Form = 4pp.

CONTENTS

THE REBATRON AS A HIGH ENERGY ACCELERATOR

I. Introduction

The electric field, that is responsible for the acceleration of charged particles can be written as the sum of an electrostatic and an inductive component. The electrostatic component is generated by electric charges and its divergence is proportional to the charge density while its curl is zero. The inductive electric field, on the other hand, is generated by a time varying magnetic field and its curl is proportional to the rate of change of magnetic field, while its divergence is zero. It is the inductive field that is responsible for the acceleration of particle in induction accelerators[1-5].

Only modest acceleration can be achieved with electrostatic fields because the maximum potential is limited by insulator flash-over. However, this is not the case with inductive fields, since the voltage is induced only in the circuit threading the flux and the voltages of a sequence of circuits successively add to the energy W of the accelerated particle. The striking difference between the two fields becomes apparent when the orbit of the particle is circular. After a complete revolution $W_2 - W_1 = 0$ for an electrostatic field, but $W_2 - W_1 \neq 0$ for an inductive field, if the magnetic flux through the particle orbit changes with time. An additional advantage of induction accelerators is their inherent low impedance. As a result, these devices are ideally suited to drive high current beams.

Quite naturally, induction accelerators are divided into linear and cyclic. The linear devices are in turn divided in Astron-type[6-9], Radlac-type[10-11], and auto-accelerators.[12,13].

Manuscript approved November 27, 1985.

In the first type, ferromagnetic induction cores are used to generate the accelerating field, while "air core" cavities are used in the second. In the auto-accelerator the air core cavities are excited by the beam's self fields rather than external fields. Similarly, cyclic accelerators can be divided into two categories. In the first category belong those cyclic accelerators that use weak focusing to confine the electron beam as in the conventional[14,15] and the modified betatron[14-16]. In the second category beam confinement is achieved with strong focusing fields. This latter category includes the Stellatron[19], Racetrack[20], and Rebatron accelerators[21]. All three devices are currently in a rather preliminary state of development. In the last two devices[20,21] the particle acceleration occurs rapidly, i.e., in a few usec and thus limitations imposed by instabilities, field errors and synchotron radiation losses are substantially relaxed.

A rebatron[21] is shown schematically in Fig. 1. The high gradient localized field that is responsible for the rapid acceleration is produced by a convoluted parallel transmission line, although other transmission lines may be more appropriate in an actual system. Since the acceleration occurs over a few usecs, the contraints imposed on the vertical field are very stringent. To reduce the inductance of the system, the vertical field is generated by two coaxial, cylindrical plates as shown in the lower right corner of Fig. 1. The axes of these plates coincide with the major axis of the toroidal vessel and are located symmetrically around the minor axis of the torus. The purpose of the gap in the outer plate is to provide a field with the desirable external field index. The transmission lines change mainly the local, vertical magnetic field, while the magnetic flux through the beam orbit remains approximately constant.

The mismatch between the beam energy and the vertical field is alleviated by a strong focusing field. This field is

generated by a set of $\ell = 2$ torsatron windings, i.e., two twisted wires that carry current in the same direction. In addition to the transverse components of the field, the torsatron windings provide a zero order toroidal magnetic field. The beneficial effect of twisted quadrupole fields on the beam orbits has been recognized for several years[22]. In recent years, the $\ell = 2$ stellarator field has been used by Roberson et al. to improve the bandwidth of the modified betatron in a device named Stellatron[19] and also in the racetrack accelerator[20], a device similar to rebatron.

In recent studies[21], we have demonstrated that the energy bandwidth of a rebatron accelerator can be very wide. In addition, we have shown that the torsatron windings also substantially improve the current carrying capabilities of the device and could alleviate the beam displacement problem associated with the diffusion of the self magnetic field. Therefore, it is expected that the limiting current in a rebatron would be determined from collective instabilities and not from the macroscopic stability on the beam orbits.

Beam capture in the rebatron, as in other devices that use strong focusing fields, is very difficult. The reason is that the strong focusing fields make the particle orbits insensitive to the energy mismatch and thus, small changes in the vertical magnetic field are not sufficient to move the beam from the injection position near the wall to the minor axis of the torus. Recently, we have developed two injection schemes that appear very promising. One is based on the drag force of a resistive chamber wall[23] and the other[24] on the modification of the beam orbit by a time varying field.

During acceleration, when the vertical magnetic field B_v exceeds by far the torsatron field B_t, the beam dynamics is solely determined by the vertical and toroidal fields. For most applications of interest $B_v >> B_t$ at the peak of acceleration and

thus, beam extraction from the rebatron is similar to that from a modified betatron[21].

In this report, we present results from our studies of the beam acceleration in a rebatron accelerator when the magnetic fields varies with time. In section II the applied electric and magnetic fields are described and in section III a simple theoretical model is examined and some important conclusions are derived from this model. The numerical results for an accelerated beam and their interpretation are given in section IV. Finally, the conclusions of this investigation are presented in section V.

II. Applied Fields

a. Torsatron and External Toroidal Magnetic Fields

In the local cylindrical coordinate system $\hat{e}_\rho$, $\hat{e}_\phi$, $\hat{e}_s$ shown in Fig. 2, the magnetic field components of the $\ell=2$ torsatron and external toroidal coils are given by the expressions[21]

$$B_\rho = B_\rho^{(o)} + B_\rho^{(1)} + B_{\rho+}^{(1)} + B_{\rho-}^{(1)}, \tag{2.1a}$$

$$B_\phi = B_\phi^{(o)} + B_\phi^{(1)} + B_{\phi+}^{(1)} + B_{\phi-}^{(1)}, \tag{2.1b}$$

$$B_s = \frac{1}{1 + (\rho/r_o)\cos\phi}\left(B_s^{(o)} + B_{s+}^{(1)} + B_{s-}^{(1)}\right) \tag{2.1c}$$

where

$$B_\rho^{(o)} = B_o \sum_{m=1}^{\infty} A_m^{(o)}\, m\tilde{\rho}_o\, I'_{2m}(m\tilde{\rho}) \sin\left[2m(\phi-\alpha s)\right], \tag{2.2a}$$

$$B_\phi^{(o)} = B_o \sum_{m=1}^{\infty} A_m^{(o)}\, 2m\, \frac{\tilde{\rho}_o}{\tilde{\rho}}\, I_{2m}(m\tilde{\rho}) \cos\left[2m(\phi-\alpha s)\right], \tag{2.2b}$$

$$B_s^{(o)} = B_{so}^{ext} + B_o\left[1 - \sum_{m=1}^{\infty} A_m^{(o)}\, m\tilde{\rho}_o\, I_{2m}(m\tilde{\rho}) \cos\left[2m(\phi-\alpha s)\right]\right], \tag{2.2c}$$

and

$$B_{\rho\pm}^{(1)} = \frac{1}{4}\frac{\rho_o}{r_o} B_o \sum_{m=1}^{\infty} \{A_m^{(1)} I'_{2m\pm1}(m\tilde{\rho}) - A_m^{(o)} [2(1\pm m) m\tilde{\rho}\, I_{2m}(m\tilde{\rho})$$

$$+ [(m\tilde{\rho})^2 + 2m(2m\pm1) + 1] I_{2m}(m\tilde{\rho})\} \sin[(2m\pm1)\phi - 2m\alpha s], \qquad (2.3a)$$

$$B_{\phi\pm}^{(1)} = \frac{1}{4}\frac{\rho_o}{r_o} B_o \sum_{m=1}^{\infty} (2m\pm1) \{A_m^{(1)} \frac{1}{m\tilde{\rho}} I_{2m\pm1}(m\tilde{\rho})$$

$$- A_m^{(o)} [m\tilde{\rho}\, I'_{2m}(m\tilde{\rho}) + (1\pm2m) I_{2m}(m\tilde{\rho})]\} \cos[(2m\pm1)\phi - 2m\alpha s] \qquad (2.3b)$$

$$B_{s\pm}^{(1)} = -\frac{1}{4}\frac{\rho_o}{r_o} B_o \sum_{m=1}^{\infty} \{ A_m^{(1)} I_{2m\pm1}(m\tilde{\rho})$$

$$- A_m^{(o)} m\tilde{\rho} [m\tilde{\rho}\, I'_{2m}(m\tilde{\rho}) + (1\pm2m) I_{2m}(m\tilde{\rho})]\} \cos[(2m\pm1)\phi - 2m\alpha s] \qquad (2.3c)$$

$$B_\rho^{(1)} = -\frac{1}{2\alpha r_o} B_o \left[\ln \frac{8r_o}{\rho_o} - \frac{1}{2}\right] \sin\phi \qquad (2.3d)$$

$$B_\phi^{(1)} = -\frac{1}{2\alpha r_o} B_o \left[\ln \frac{8r_o}{\rho_o} - \frac{1}{2}\right] \cos\phi \qquad (2.3e)$$

The coefficients $A_m^{(o)}$ and $A_m^{(1)}$ are equal to

$$A_m^{(o)} = K'_{2m}(m\tilde{\rho}_o)\, C_m , \qquad (2.4a)$$

$$A_m^{(1)} = [(m\tilde{\rho}_o)^2 K'_{2m}(m\tilde{\rho}_o) - K_{2m\pm1}(m\tilde{\rho}_o) + (1\pm4m)(m\tilde{\rho}_o) K'_{2m}(m\tilde{\rho}_o)] C_m , \qquad (2.4b)$$

where

$$C_m = \frac{2\sin(2m\delta)}{2m\delta} . \qquad (2.5)$$

The remaining parameters are defined as follows:

$$B_o = \frac{8 \pi I_o}{c L} \quad , \tag{2.6}$$

$$\alpha = \frac{2 \pi}{L} \quad , \tag{2.7}$$

$$\tilde{\rho} = 2 \alpha \rho \quad , \tag{2.8a}$$

$$\tilde{\rho}_o = 2 \alpha \rho_o \quad . \tag{2.8b}$$

Here, I_o is the current flowing in the windings, ρ_o is the winding radius and L is the period of the windings, $2 \delta \rho_o$ is the width of the current carrying conductor, r_o is the major radius of the torus, B_{so}^{ext} is the external toroidal magnetic field at the minor axis of the torus and $I_n(x)$, $K_n(x)$, $I_n'(x)$, $K_n'(x)$ are the modified Bessel functions of the first and second kind and their derivatives. In a toroidal device, the period satisfies the relation

$$\frac{2 \pi r_o}{L} = N \quad , \tag{2.9}$$

where N is the number of turns around the torus for each winding. The zero order fields $B_\rho^{(o)}$, $B_\phi^{(o)}$, $B_s^{(o)}$ are the field components produced by the helical windings in a straight (cylindrical) configuration while the terms proportional to ρ_o/r_o are the first order toroidal corrections. These fields, as given by Eqs. (2.2) and (2.3), have been obtained for the surface current density

$$J_\rho = 0 \tag{2.10a}$$

$$J_\phi = \frac{I_o}{2\delta\rho_o} \frac{\alpha o_o}{1 + (\rho/r_o)\cos\phi} f(\phi - \alpha s), \tag{2.10b}$$

$$J_s = \frac{I_o}{2\delta\rho_o} f(\phi - \alpha s), \tag{2.10c}$$

where $f(\phi)$ is a periodic function of ϕ with period π, and

$$f(\phi) = \begin{matrix} 1 \text{ if } -\delta < \phi < \delta \\ 0 \text{ if } \delta < \phi < \pi - \delta \end{matrix} . \tag{2.11}$$

From Eqs. (2.3d) and (2.3e) it follows that there is a constant $B_z^{(1)}$ component of the torsatron magnetic field. This component is due to the fact that the currents in the two torsatron windings are in the same direction. (In a stelarator this component is zero). It is assumed, in the rest of this paper, that this undesirable component is cancelled by adding an external magnetic field.

The three magnetic components at s=0 are plotted in Figs. 3a and 3b, for $\phi = 0$ and $\phi = \pi/2$, respectively. The various parameters for these plots are listed in Table I and are those used for the torsatron and external toroidal magnetic field in the following sections. At $\phi = 0$, the B_ρ component is equal to zero. The B_ϕ component increases linearly with ρ near the minor axis and much faster near the windings. The toroidal correction at $\rho = 0$ is approximately -100 Gauss. In Fig. 3, in addition to the toroidal field produced by the torsatron windings, there is an external toroidal field B_s^{ext} equal to 10 kG at $\rho = 0$, which is produced by a set of toroidal coils. As seen from Eqs.

(2.1c) and (2.2c) this field varies as $1/r$ and is independent of the toroidal angle $\theta = -s/r_o$. At $\rho = 0$, the total toroidal field $B_s = B_{so}^{ext} + B_o = 15.6$ kG. In general, B_s does not vary as $1/r$, since it depends on the toroidal angle.

Figure 3c gives the magnetic field lines in the (r,z) and (ρ,s) planes. Because of the toroidal corrections, the magnetic axis does not coincide with the minor axis of the torus, located at r=100 cm. The magnetic axis is always shifted toward the major axis of the torus. This shift is due to the contribution in the magnetic field, at some point inside the torus, mainly from that section of the windings which is located at a toroidal angle 180° from this point.

In the theoretical model that is formulated in Section III, the toroidal corrections are neglected as well as all the terms with $m > 2$ in Eq. (2.1) through (2.4). Also, it is assumed that $\delta << 1$, so that $C_1 = 2$. Finally, use is made of the cylindrical components B_r, B_θ, B_z in the global coordinate system $\hat{e}_r$, $\hat{e}_\theta$, $\hat{e}_z$ shown in Fig. 2. Their relation to the magnetic components in the local coordinate system $\hat{e}_\rho$, $\hat{e}_\phi$, $\hat{e}_s$ is as follows

$$B_r = B_\rho \cos\phi - B_\phi \sin\phi, \tag{2.12a}$$

$$B_z = B_\rho \sin\phi + B_\phi \cos\phi, \tag{2.12b}$$

$$B_\theta = -B_s . \tag{2.12c}$$

Under these conditions, the magnetic field from the torsatron and the toroidal coils is approximately equal to

$$B_r \approx B_0 \varepsilon_1 \left[I_1(\tilde{\rho}) \sin(\phi - 2\alpha s) + I_3(\tilde{\rho}) \sin(3\phi - 2\alpha s) \right], \qquad (2.13a)$$

$$B_z \approx B_0 \varepsilon_1 \left[I_1(\tilde{\rho}) \cos(\phi - 2\alpha s) - I_3(\tilde{\rho}) \cos(3\phi - 2\alpha s) \right], \qquad (2.13b)$$

$$B_\theta \approx B_{\theta o} + 2 B_0 \varepsilon_1 I_2(\tilde{\rho}) \cos(2\phi - 2\alpha s) \qquad (2.13c)$$

where

$$\varepsilon_1 = \tilde{\rho}_0 K_2'(\tilde{\rho}_0), \qquad (2.14a)$$

$$B_{\theta o} = - B_{so}^{ext} - B_0. \qquad (2.14b)$$

Eqs. (2.1) through (2.8) were used to compute the magnetic field in the numerical integration of the equations of motion for the beam centroid. In this case too, it was assumed that $\delta \ll 1$, so that $C_1 = 2$ and, in order to save computer time, only one term, namely $m = 1$, was retained in the series.

b. Vector Potential and Magnetic Field of the Plates.

Let a single cylindrical plate of width b and height h, where $b \ll h$, be located so that the axis of the cylinder coincides with the major axis of the torus and the distance of the plate from the minor axis of the torus be equal to a. For a homogeneous current density with a single component $J_\theta = I_p/(bh)$, where I_p is the current flowing in the plate, the vector potential A_θ is[25]

$$A_\theta = \frac{I_p}{c} \hat{A}_\theta \quad , \qquad (2.15)$$

where

$$\hat{A}_\theta\ (x,z,r_o,a,h,b) =$$

$$= \frac{4}{bh} \int_{a-\frac{b}{2}}^{a+\frac{b}{2}} dx' \int_{-h/2}^{h/2} dz' \frac{\left(\frac{r_o + x'}{r_o + x}\right)^{1/2}}{\sqrt{1 - k'^2}} \left[\frac{1}{2}\ (1+k'^2)\ K'(k') - E'(k')\right], \tag{2.16a}$$

and

$$k'^2 = \frac{(x - x')^2 + (z - z')^2}{(2\ r_o + x + x')^2 + (z - z')^2}\ . \tag{2.16b}$$

The point (x,z), where $\hat{A}_\theta$ is computed, is in the local coordinate system $\hat{e}_x$, $\hat{e}_z$, $\hat{e}_s$ of Fig. 2, and $K'(k')$, $E'(k')$ are the complete elliptic integrals. When the plate is located close to the torus, so that $a/r_o << 1$, and one is interested in the vector potential only inside the torus, then $k'^2 << 1$ and the elliptic integrals can be expanded[26] with respect to k'^2. To lowest order $\hat{A}_\theta$ is given by

$$\hat{A}_\theta(x,\ z,\ r_o,\ a,\ h,\ b) \approx \tag{2.17}$$

$$\approx -\frac{2}{bh} \int_{a-\frac{b}{2}}^{a+\frac{b}{2}} dx' \int_{-h/2}^{h/2} dz' \left(\frac{r_o + x'}{r_o + x}\right)^{1/2} \left(\frac{1}{2}\ \ell n\ \frac{k'^2}{16} + 2\right)$$

$$\approx -\frac{2}{bh} \int_{a-\frac{b}{2}}^{a+\frac{b}{2}} dx' \int_{-h/2}^{h/2} dz' \left[-\frac{1}{2}\ \frac{x' + x}{r_o}\right.$$

$$\left. + \left(1 + \frac{1}{2}\ \frac{x' - x}{r_o}\right) \left[\frac{1}{2}\ \ell n\ \frac{(x' - x)^2 + (z' - z)^2}{(8r_o)^2} + 2\right]\right],$$

which contains the toroidal corrections to the lowest order in a/r_o. A further simplication occurs from the fact that $b \ll h$, so that $\hat{A}_\theta$ is computed in the limit $b \to 0$. Then the integrals in Eq. (2.17) can be computed exactly and $\hat{A}_\theta$ is equal to

$$\hat{A}_\theta\ (x,\ z,\ r_o,\ a,\ h,\ 0) = \frac{a + x}{r_o} \tag{2.18}$$

$$-2\ \left(1 + \frac{1}{2}\,\frac{a - x}{r_o}\right)\left[1 + \frac{a - x}{h}\left(\text{Arctan}\,\frac{\frac{h}{2} + z}{a - x} + \text{Arctan}\,\frac{\frac{h}{2} - z}{a - x}\right)\right.$$

$$\left. + \frac{1}{2}\,\frac{\frac{h}{2} + z}{h}\,\ell n\,\frac{\left(\frac{h}{2} + z\right)^2 + (a - x)^2}{(8r_o)^2} + \frac{1}{2}\,\frac{\frac{h}{2} - z}{h}\,\ell n\,\frac{\left(\frac{h}{2} - z\right)^2 + (a - x)^2}{(8r_o)^2}\right].$$

The B_r, B_z components of the magnetic field near the plate (and therefore inside the torus), and to the lowest order in a/r_o, are equal to

$$B_r = \frac{I_p}{c}\,\hat{B}_r \quad , \tag{2.19a}$$

$$B_z = \frac{I_p}{c}\,\hat{B}_z \quad , \tag{2.19b}$$

where

$$\hat{B}_r = -\frac{\partial \hat{A}_\theta}{\partial z} \quad , \tag{2.20a}$$

$$\hat{B}_z = \frac{\partial \hat{A}_\theta}{\partial x} + \frac{1}{r_o}\hat{A}_\theta \quad . \tag{2.20b}$$

Substitution of Eq. (2.18) into Eqs. (2.20a), (2.20b), leads to the expressions

$$\hat{B}_r = \frac{1}{h}\left(1 + \frac{1}{2}\frac{a-x}{r_o}\right) \ell n \frac{\left(\frac{h}{2}+z\right)^2 + (a-x)^2}{\left(\frac{h}{2}-z\right)^2 + (a-x)^2} \quad , \tag{2.21a}$$

and

$$\hat{B}_z = \frac{2}{h}\left[\text{Arctan}\frac{\frac{h}{2}+z}{a-x} + \text{Arctan}\frac{\frac{h}{2}-z}{a-x}\right] \tag{2.21b}$$

$$-\frac{1}{2r_o}\left[\frac{\frac{h}{2}+z}{h}\ell n\frac{\left(\frac{h}{2}+z\right)^2 + (a-x)^2}{(8r_o)^2} + \frac{\frac{h}{2}-z}{h}\ell n\frac{\left(\frac{h}{2}-z\right)^2 + (a-x)^2}{(8r_o)^2}\right].$$

In the limit $r_o \to \infty$, Eqs. (2.20), (2.21) reduce to the magnetic field of an infinite length slab, as they should.

The particle orbits are not stable unless the external field index n of the vertical magnetic field is in the region $0 < n < 1$. Such a field can be generated by a set of two plates which surround the torus (cf. Fig. 1), with the outer plate having a gap symmetrically located in the middle of the plate. From the vector potential for a single plate, it is easy to compute the vector potential of the outer plate with a gap of height H_o. This vector potential is given by

$$\hat{A}_{\theta+} = \frac{h}{h - H_o} \hat{A}_\theta(x,z,r_o,a,h,0) - \frac{H_o}{h - H_o} \hat{A}_\theta(x,z,r_o,a,H_o,0). \quad (2.22a)$$

The current density in the presence of a gap is proportional to $I_p/(h - H_o)$. The first term in Eq. (2.22a) is the contribution to $\hat{A}_{\theta+}$ from the whole plate (of height h) and the second term is the contribution of the gap (of height H_o) which should be subtracted. Since the inner plate is located at a distance -a from the minor axis and carries a current $- I_p$, its vector potential is

$$\hat{A}_{\theta-} = - \hat{A}_\theta(x,z,r_o,-a,h,0) , \quad (2.22b)$$

and the combined potential from both plates is

$$A_\theta = \frac{I_p}{c} (\hat{A}_{\theta+} + \hat{A}_{\theta-}). \quad (2.23)$$

The magnetic field is computed with the help of Eqs. (2.13) through (2.23). Near the minor axis, the magnetic field simplifies to the following linearized expressions:

$$B_r = - B_{zo} n_o \frac{z}{r_o} , \quad (2.24a)$$

$$B_z = B_{zo} (1 - n_o \frac{x}{r_o}) , \quad (2.24b)$$

where

$$n_o \equiv - \frac{r_o}{B_{zo}} \left(\frac{\partial B_z}{\partial x}\right)_{\substack{x=0 \\ z=0}} , \quad (2.25a)$$

$$\equiv - \frac{r_o}{B_{zo}} \left(\frac{\partial B_r}{\partial z}\right)_{\substack{x=0 \\ z=0}}$$

$$= \frac{\frac{r_o}{2a}\frac{H_o}{2a}\frac{h}{2a}\left(1+\frac{1}{2}\frac{a}{r_o}\right)\left(1+\frac{H_o}{h}\right)-\frac{1}{2}}{\text{Arctan}\,\frac{h}{2a}} \quad \frac{\frac{h}{2a}}{1+\left(\frac{h}{2a}\right)^2} \,,$$

$$B_{zo} = \frac{I_p}{c}\hat{B}_{zo} \,, \tag{2.25b}$$

$$\hat{B}_{zo} = \frac{8}{h}\,\text{Arctan}\,\frac{h}{2a} + \frac{H_o}{h-H_o}\left(\frac{4}{h}\,\text{Arctan}\,\frac{h}{2a}\right.$$

$$\left. - \frac{4}{H_o}\,\text{Arctan}\,\frac{H_o}{2a} - \frac{1}{2r_o}\,\ell n\,\frac{1+\left(\frac{h}{2a}\right)^2}{1+\left(\frac{H_o}{2a}\right)^2}\right) . \tag{2.25c}$$

Equations (2.24a), (2.24b) are identical in form to the linearized betatron field in the modified betatron. According to Eq. (2.25a) the external field index n_o at x=z=0 is sensitive to the height H_o of the gap. In particular, if there is no gap on the outer plate (i.e., $H_o = 0$), then n_o becomes negative.

The magnetic field components of the plates are plotted without a gap in Fig. 4 and with a gap on the outer plate in Fig. 5. The various parameters for these plots are listed in Table II. The effect of the gap on the magnetic field is quite prominent. In the absence of a gap, n_o changes from positive to negative as r increases from 90 to 110 cm for z less than 10 cm. On the other hand, when the gap is present, n_o has the desired value of 0.5 near the minor axis of the torus (i.e., in the linear regime), but as one approaches the gap, n_o varies from positive to negative as z increases from zero to 10 cm. Figures 4b, 5b and 4d, 5d show the variation of B_r versus r and B_z versus z, respectively, for various values of z or r. Ideally, they should be straight lines, parallel to the horizontal axis in the region of interest. As may be seen from Fig. 5 this is the case when there is a gap. Although only the first order toroidal

corrections were retained, they are quite noticeable. For example, in Fig. 4a at z=0, there is a difference of 0.6 Gauss/kA in the values of B_z at r=90 cm and r=110 cm, due to the toroidal correction. Finally, it should be pointed out that, because of the gap, the value of the vertical magnetic field at the minor axis drops from 18.45 Gauss/kA to 17.58 Gauss/kA.

As already mentioned, in order to keep the beam matched, the current in the plates should increase in synchronism with the energy of the beam. Therefore, there is an electric field E_p associated with the time dependent vector potential of the plates, namely

$$E_p = -\frac{1}{c}\frac{\partial A_\theta}{\partial t} = -\frac{\dot{I}_p}{c^2}\left(\hat{A}_{\theta+} + \hat{A}_{\theta-}\right). \tag{2.26}$$

As shown in Section III, this electric field will have an effect on the rate of change of the current in the plates.

C. The Accelerating Electric Field.

Consider a periodic sequence of cylindrical perfectly conducting sections of radius ρ_w with their axes lying along the same line and separated by a distance d, as shown in Fig. 6a. Each alternate section is charged to a potential $+V_0/2$ and the remaining sections are charged to a potential $-V_0/2$. The period of the structure is equal to D, where D >> d. Under this assumption, the local electric field in the region $-D/4 < s < D/4$ is, for all practical purposes, the same as that of two cylinders of infinite extent. In either case, the local

electric field is given by the solution of Laplace's equation, i.e., $\Delta V = 0$. The advantage of solving this equation for the periodic structure rather than the two cylinders of infinite extent is that it leads to a solution expressed in terms of a much faster converging series. The lowest order toroidal corrections have been included in the solution. The method for incorporating these corrections is the same as that used for the torsatron magnetic field. The operator Δ in the local coordinate system $\hat{e}_\rho$, $\hat{e}_\phi$, $\hat{e}_s$ can be written as follows:

$$\Delta = \Delta^{(0)} + \delta\Delta \tag{2.27}$$

where

$$\Delta^{(0)} = \frac{1}{\rho} \frac{\partial}{\partial \rho} \rho \frac{\partial}{\partial \rho} + \frac{1}{\rho^2} \frac{\partial^2}{\partial \phi^2} + \frac{\partial^2}{\partial s^2} \quad , \tag{2.28a}$$

$$\delta\Delta = \frac{1}{r_o} \left(\rho \cos\phi \frac{\partial^2}{\partial s^2} - \frac{1}{\rho} \frac{\partial}{\partial \rho} \rho^2 \cos\phi \frac{\partial}{\partial \rho} - \frac{1}{\rho} \frac{\partial}{\partial \phi} \cos\phi \frac{\partial}{\partial \phi} \right), \tag{2.28b}$$

and $s = - r_o \theta$. The potential V is also written as a sum of the zero order and first order contribution in the toroidal corrections, namely, $V = V^{(0)} + V^{(1)}$, where $V^{(0)}$ satisfies the zero order Laplace equation

$$\Delta^{(0)} V^{(0)} = 0 \quad . \tag{2.29}$$

Since the orginal Laplace equation becomes equal to

$$(\Delta^{(0)} + \delta\Delta)\ (V^{(0)} + V^{(1)}) = 0, \qquad (2.30a)$$

it follows from Eq. (2.29) that the first order toroidal correction in the potential $V^{(1)}$ satisfies the equation

$$\Delta^{(0)}\ V^{(1)} = -\ \delta\Delta\ V^{(0)}. \qquad (2.30b)$$

The method of computing the toroidal corrections consists in solving first Eq. (2.29) with the boundary condition at $\rho = \rho_w$:

$$V^{(0)} = \begin{cases} \frac{V_o}{d}\, s & \text{if} \quad 0 < s < \frac{d}{2} \\ \frac{V_o}{2} & \text{if} \quad \frac{d}{2} < s < \frac{D-d}{2} \\ \frac{V_o}{2}\left(\frac{D}{2} - s\right) & \text{if} \quad \frac{D-d}{2} < s < \frac{D}{2} \end{cases}, \qquad (2.31)$$

and $V^{(0)}(-s) = -\ V^{(0)}(s)$. Then $V^{(1)}$ is computed by solving Eq. (2.30) with the boundary condition that at $\rho = \rho_w$, $V^{(1)} = 0$, if $-D/2 < s < D/2$. The accelerating electric field, being the gradient of -V, is computed from the relations

$$E_\rho = -\frac{\partial}{\partial \rho}\ (V^{(0)} + V^{(1)}) \quad , \qquad (2.32a)$$

$$E_\phi = -\frac{1}{\rho}\frac{\partial}{\partial \phi}\ (V^{(0)} + V^{(1)}) \quad , \qquad (2.32b)$$

$$E_s = -\frac{1}{1 + (\rho/r_o)\cos\phi}\ \frac{\partial}{\partial s}\ (V^{(0)} + V^{(1)}) \ . \qquad (2.32c)$$

The components of the accelerating electric field, including the lowest order toroidal corrections, are

$$E_\rho = E_\rho^{(0)} + E_\rho^{(1)} \quad , \tag{2.33a}$$

$$E_\phi = E_\phi^{(1)} \quad , \tag{2.33b}$$

$$E_s = \frac{1}{1 + (\rho/r_0)\cos\phi} \left[E_s^{(0)} + E_s^{(1)}\right], \tag{2.33c}$$

where

$$E_\rho^{(0)} = - \sum_{n=1}^{\infty} A_n^{(0)} I_1(\tilde{\rho}_n) \sin(\tilde{s}_n) \quad , \tag{2.34a}$$

$$E_s^{(0)} = \sum_{n=1}^{\infty} A_n^{(0)} I_0(\tilde{\rho}_n) \cos(\tilde{s}_n) \quad . \tag{2.34b}$$

and

$$E_\rho^{(1)} = - \cos\phi \sum_{n=1}^{\infty} \left\{ A_n^{(1)} \left[I_0(\tilde{\rho}_n) - \frac{1}{\tilde{\rho}_n} I_1(\tilde{\rho}_n)\right] + B_n^{(1)} \left[\left(1 + \tilde{\rho}_n^2\right) I_0(\tilde{\rho}_n) + 2\,\tilde{\rho}_n I_1(\tilde{\rho}_n)\right] \right\} \sin(\tilde{s}_n) \quad , \tag{2.35a}$$

$$E_\phi^{(1)} = \sin\phi \sum_{n=1}^{\infty} \left\{ A_n^{(1)} \frac{1}{\tilde{\rho}_n} I_1(\tilde{\rho}_n) + B_n^{(1)} \left[I_0(\tilde{\rho}_n) + \tilde{\rho}_n I_1(\tilde{\rho}_n)\right] \right\} \sin(\tilde{s}_n) \quad , \tag{2.35b}$$

$$E_s^{(1)} = -\cos\phi \sum_{n=1}^{\infty} \left[A_n^{(1)} I_1(\tilde{\rho}_n) + B_n^{(1)} \tilde{\rho}_n \left[I_0(\tilde{\rho}_n) + \tilde{\rho}_n I_1(\tilde{\rho}_n) \right] \right] \cos(\tilde{s}_n) \ . \qquad (2.35c)$$

The rest of the parameters in these relations are defined as follows:

$$A_n^{(0)} = 2 \frac{V_o}{D/2} \frac{\sin (2n-1) \pi \frac{d}{D}}{(2n-1) \pi \frac{d}{D}} \frac{1}{I_0\left[(2n-1) \pi \frac{\rho_w}{D/2}\right]} \ , \qquad (2.36a)$$

$$A_n^{(1)} = \frac{1}{2} \frac{\rho_w}{r_o} \left[(2m-1) \pi \frac{\rho_w}{D/2} + \frac{I_0\left[(2m-1) \pi \frac{\rho_w}{D/2}\right]}{I_1\left[(2m-1) \pi \frac{\rho_w}{D/2}\right]} \right] A_n^{(0)} \ , \qquad (2.36b)$$

$$B_n^{(1)} = -\frac{1}{2} \frac{\rho_w}{r_o} \frac{1}{(2n-1) \pi \frac{\rho_w}{D/2}} A_n^{(0)} \ , \qquad (2.36c)$$

and

$$\tilde{\rho}_n = (2n-1) \pi \frac{\rho}{D/2} \ , \qquad (2.37a)$$

$$\tilde{s}_n = (2n-1) \pi \frac{s}{D/2} \ . \qquad (2.37b)$$

The electric field is computed in the interval $-D/4 < s < D/4$. A choice of $D/4 \approx 3\rho_w$ leads to a fairly accurate representation of the accelerating field. As a result of the modified Bessel functions, the series in Eqs. (2.34) and (2.35) converge considerably faster than those used previously[21]. It may also be seen from these equations that as ρ increases from zero to ρ_w more terms must be retained in the series for convergence. Finally, the presence of the toroidal corrections

and, in particular, the 1/r dependence of the s-component of the electric field (cf. Eq. (2.33c)), is essential in the orbit equations. It will be shown in Section III that the toroidal corrections of the accelerating electric field cancel out the first order contribution from the electric field of the plates (Eq. (2.26)) in the expression for the mismatch $\delta\gamma/\gamma$, and as a consequence the drift of the particle orbits is, for all practical purposes, zero.

The electric field lines and field components, given by Eq. (2.33) through (2.37) are plotted in figs. 6b, 6c and 6d. The various parameters for these plots are listed in Table III. The dotted lines in Fig. 6b indicate the location of the accelerating gap. Fifty one terms have been retained in the series. In Fig. 6c, the Gibbs phenomenon is quite noticeable at $\rho = \rho_w = 10$ cm, where the E_s component is discontinuous. As expected, the line integral along the s-axis and at any radius ρ is equal to V_0. As may be seen from Fig. 6d the E_ρ component changes sign as s increases, and therefore, on the average it has little effect on the particle orbits. The poloidal component E_ϕ was not plotted since it is zero at $\phi = 0$. In general it is small and its contribution to the particle orbits is negligible.

The electric fields given above are a good representation of the fields produced inside the torus by a transmission line, since in this region the inductive magnetic field is zero and therefore the potential is described by $\Delta V = 0$.

III. Simple Theoretical Model

a. Approximate Equations of Motion and Conservation Law

The exact equations of motion are too complicated to provide any insight into the effect that the torsatron and vertical magnetic fields have on the particle orbits. A better

understanding is gained by a simple model which provides fairly accurate results and is based on the assumption that the toroidal velocity v_θ of the particle, being very close to the velocity of light, remains constant (but not the energy). In this case

$$s = v_\theta t \ , \tag{3.1}$$

and the remaining equations of the motion are

$$\frac{d}{dt}(\gamma \dot{r}) - \gamma r \dot{\vartheta}^2 = - \frac{e}{mc} (v_\vartheta B_z - \dot{z} B_\theta) \ , \tag{3.2a}$$

$$\frac{d}{dt}(\gamma \dot{z}) = - \frac{e}{mc} (\dot{r} B_\theta - v_\vartheta B_r). \tag{3.2b}$$

For simplicity, the self fields will be neglected in the present analysis. Also, the magnetic field of the torsatron and toroidal coils is given by the simplified Eqs. (2.13) and that of the plates by Eqs. (2.24). In Eqs. (2.13), $2\alpha s$ is replaced by $- \omega_w t$ (cf. Eq. (3.1)),

where

$$\omega_w = 2 \alpha v_\theta. \tag{3.3}$$

Set $x = r - r_o$, and define the complex amplitude

$$u = x + i z = o e^{i\phi}. \tag{3.4}$$

Then Eqs. (3.2a), (3.2b) can be combined into one complex

equation of motion, namely,

$$\ddot{u} + i \left(\frac{\Omega_{\theta o}}{\gamma} + 2\varepsilon_1 \frac{\Omega_o}{\gamma} I_2(\tilde{\rho}) \cos (2\phi + \omega_w t) - i \frac{\dot{\gamma}}{\gamma} \right) \dot{u}$$

$$+ \varepsilon_1 \omega_w \frac{\Omega_o}{\gamma} \left(I_1(\tilde{\rho})\, e^{-i(\phi+\omega_w t)} - I_3(\tilde{\rho})\, e^{i(3\phi+\omega_w t)} \right)$$

$$+ \omega_\perp^2 u + \delta\omega^2 u^* = v_\theta \left(\frac{v_\theta}{r_o} - \frac{\Omega_{zo}}{\gamma} \right), \qquad (3.5)$$

where

$$\omega_\perp^2 = \frac{1}{2} \omega_o^2, \qquad (3.6a)$$

$$\delta\omega^2 = \frac{1}{2} \omega_o^2 - n_o \frac{v_\theta}{r_o} \frac{\Omega_{zo}}{\gamma}, \qquad (3.6b)$$

$$\omega_o = \frac{v_\theta}{r_o}, \qquad (3.6c)$$

and $\Omega_{\theta o}$, Ω_o, Ω_{zo} are the nonrelativistic cyclotron frequencies associated with the magnetic fields $B_{\theta o}$, B_o, B_{zo} (i.e., $\Omega = (e/mc)\, B$). The quantity $2\pi/\omega_o$ is the time it takes a particle on the minor axis to make one revolution around the torus. Moreover, the rate of change of γ is mainly due to the s-components of the electric fields of the transmission line and the plates, so that

$$\dot{\gamma} = - \frac{e}{mc^2} v_\theta \left(E_{gap} + E_p \right), \qquad (3.7)$$

where $E_{gap} = - E_s$, and E_s, E_p are given by Eqs. (2.33c), (2.26), respectively.

Equation (3.5) is still too difficult to handle. But it leads to a conservation law when the fast motion which oscillates with frequency ω_w is averaged out in Eq. (3.5). Details may be found elsewhere[24]. Only the final result will be given here which was obtained under the assumptions that γ remains constant and that $\omega_w << |\Omega_{\theta 0}|/\gamma$. Under these conditions the conservation law becomes

$$\left(1 - n_0\left(1 - \frac{\delta\gamma}{\gamma}\right)\right)\left(\frac{X}{r_0} - \frac{\delta\gamma/\gamma}{1 - n_0\left(1 - \frac{\delta\gamma}{\gamma}\right)}\right)^2 + n_0\left(1 - \frac{\delta\gamma}{\gamma}\right)\left(\frac{Z}{r_0}\right)^2$$

$$+ \left(\frac{\omega_0}{\omega_w}\right)^2 \left(b_- I_1^2(2\alpha R) + b_+ I_3^2(2\alpha R)\right) = K, \qquad (3.8)$$

where

$$\frac{\delta\gamma}{\gamma} = \frac{\gamma - \gamma_0}{\gamma}, \qquad (3.9a)$$

$$\gamma_0 = \frac{\Omega_{z0} r_0}{v_\theta}, \qquad (3.9b)$$

$$b_\pm = \frac{\left(\varepsilon_1 \frac{B_0}{B_{z0}}\right)^2 \left(1 - \frac{\delta\gamma}{\gamma}\right)^2}{1 \pm \frac{\omega_0}{\omega_w} \frac{B_{\theta 0}}{B_{z0}} \left(1 - \frac{\delta\gamma}{\gamma}\right)}. \qquad (3.9c)$$

Here, K is the constant of integration and is determined from the initial conditions, (X,Z) is the average (or guiding center) position of the beam centroid, $R = (X^2 + Z^2)^{1/2}$, γ_0 is the value of γ that matches the vertical magnetic field B_z from the plates when the beam centroid is at X = Z = 0 (i.e., at the origin of the local coordinate system), and $\delta\gamma/\gamma$ is the mismatch between

the actual value of γ and γ_0. When the mismatch is equal to zero, then the beam is matched at the origin, i.e., the point X = Z = 0 is an equilibrium position.

Consider the special case when $2\alpha R \ll 1$ and $\delta\gamma/\gamma \ll 1$. Then Eq. (3.8), which is actually an equation for the particle orbits, simplifies to the following expression:

$$(b_- + 1 - n_0)\left(\frac{X}{r_0} - \frac{\delta\gamma/\gamma}{b_- + 1 - n_0}\right)^2 + (b_- + n_0)\left(\frac{Z}{r_0}\right)^2 = K', \quad (3.10)$$

where K' is a new integration constant. This equation describes either an ellipse or a hyperbola centered at $(\Delta r, 0)$, where

$$\frac{\Delta r}{r_0} = \frac{\delta\gamma/\gamma}{b_- + 1 - n_0} . \quad (3.11)$$

At the initial stage of the acceleration, the torsatron magnetic field B_0 is much larger than the vertical magnetic field B_{z0}, i.e., $|B_0/B_{z0}| \gg 1$. Since the external field index n_0 is of order one, it follows that $|b_-|$ is much greater than one, or $|n_0|$, or $|1 - n_0|$, and Eq. (3.10) simplifies to the relation

$$\left(\frac{X}{r_0} - \frac{\delta\gamma/\gamma}{b_-}\right)^2 + \left(\frac{Z}{r_0}\right)^2 = K' . \quad (3.12)$$

It is seen then that, in the presence of the torsatron field, at the initial stage of the acceleration the orbits on the (r,z) plane are circles centered at

$$\frac{\Delta r}{r_0} = \frac{\delta\gamma/\gamma}{b_-} . \quad (3.13)$$

This orbit displacement is independent of the external field index n_0 and since $|b_-| \gg 1$, it is not sensitive to the value of the mismatch $\delta\gamma/\gamma$, i.e., the torsatron field, which dominates at the initial stage of the acceleration, does provide confinement of the beam inside the torus.

At a later stage of the acceleration, as the vertical magnetic field increases in synchronism with the energy of the beam, it becomes eventually greater than B_0 and the condition $|b_-| << 1$ holds. In this case, Eq. (3.10) reduces to the expression

$$(1 - n_0)\left(\frac{X}{r_0} - \frac{\delta\gamma/\gamma}{1 - n_0}\right)^2 + n_0\left(\frac{Z}{r_0}\right)^2 = K' \quad . \tag{3.14}$$

Therefore, in order to have closed orbits during the whole duration of the acceleration, the condition $0 < n_0 < 1$ must be satisfied, and it is this condition that requires the presence of a gap on the outer plate, as indicated in Section II. Also, in this case

$$\frac{\Delta r}{r_0} \approx \frac{\delta\gamma/\gamma}{1 - n_0} \quad , \tag{3.15}$$

which is sensitive to the mismatch $\delta\gamma/\gamma$ and to the external field index n_0. In the special case, when $n_0 = 0$, the orbits are given by the relation X = constant, i.e., they describe a vertical motion and this may provide a possible means of extracting the beam from the toroidal chamber.

b. Rate of Change of the Current in the Plates

As mentioned in the previous Sections, the two coaxial cylindrical plates generate a local vertical magnetic field which increases in synchronism with the beam energy so that the major radius of the ring remains approximately constant. From Eq. (3.7), a particle at the origin of the local coordinate system $\hat{e}_\rho$, $\hat{e}_\phi$, $\hat{e}_s$, will gain energy at the rate

$$\dot{\gamma} \approx - \frac{e}{mc}\left[\frac{V_0}{2\pi r_0} - \frac{\dot{I}_p}{c^2}\hat{A}_{\theta 0}\right] \quad , \tag{3.16}$$

Equation (3.16) has been derived from Eqs. (2.15), (2.26) and by taking the average accelerating field in the gap equal to $E_{gap} = V_o/(2\pi r_o)$. The quantity $\hat{A}_{\vartheta o}$ is equal to

$$\hat{A}_{\vartheta o} = \frac{a}{r_o}\left[\ell n \frac{(\frac{8r_o}{a})^2}{1 + (\frac{h}{2a})^2} - \frac{4a}{h}\,\mathrm{Arctan}\,\frac{h}{2a}\right]$$

$$- 2\,\frac{H_o}{h - H_o}\left(1 + \frac{1}{2}\,\frac{a}{r_o}\right)\left[\frac{2a}{h}\,\mathrm{Arctan}\,\frac{h}{2a} - \frac{2a}{H_o}\,\mathrm{Arctan}\,\frac{H_o}{2a}\right.$$

$$\left. + \frac{1}{2}\,\ell n \frac{1 + (\frac{h}{2a})^2}{1 + (\frac{H_o}{2a})^2}\right] . \qquad (3.17)$$

The beam will remain matched at the origin during the acceleration when (cf. Eqs. (3.9b), (2.25b), (2.25c))

$$\dot{\gamma} = \frac{\dot{I}_p}{c^2}\,\frac{e}{mc}\,\hat{B}_{zo} r_o . \qquad (3.18)$$

From Eqs. (3.16), (3.18), it follows that the rate of change of the current in the plates should be equal to

$$\frac{1}{c^2}\,\dot{I}_p = - \frac{V_o}{2\pi r_o^2}\,\frac{n_p}{\hat{B}_{zo}} , \qquad (3.19a)$$

where

$$\eta_p = \frac{1}{1 - \frac{1}{r_o}\frac{\hat{A}_{\theta o}}{\hat{B}_{zo}}} \qquad (3.19b)$$

The parameter η_p is the acceleration correction factor due to the electric field of the plates and has been listed in Table II.

It is interesting to show that even when the beam centroid is slightly off the origin at some later time, the mismatch $\delta\gamma$ is still zero to first order in the displacement from the origin, if $\delta\gamma$ was initially zero. A qualitative argument will be presented here and a more precise proof is given in the Appendix. If the beam is at some position $r = r_o + x$, the average accelerating field is equal to $E_{gap} = V_o/(2\pi r)$ and the vector potential at that position is proportional to $\hat{A}_{\theta o} + (\partial \hat{A}_\theta/\partial x)\, x$, where the partial derivative is evaluated at the origin. Therefore, from Eqs. (3.9a), (3.9b) and (3.7), it follows that

$$\frac{d\delta\gamma}{dt} = -\frac{e}{mc}\left[\frac{V_o}{2\pi(r_o + x)} - \frac{\dot{I}_p}{c^2}\left(\hat{A}_{\theta o} + \frac{\partial \hat{A}_\theta}{\partial x}\right) + \frac{\dot{I}_p}{c^2}\hat{B}_{zo} r_o\right]$$

$$= -\frac{e}{mc}\left[\frac{V_o}{2\pi r_o} + \frac{\dot{I}_p}{c^2} r_o\left(\hat{B}_{zo} - \frac{1}{r_o}\hat{A}_{\theta o}\right) - \left(\frac{V_o}{2\pi r_o^2} + \frac{\dot{I}_p}{c^2}\frac{\partial \hat{A}_\theta}{\partial x}\right)x\right] = 0 \qquad (3.20)$$

In deriving Eq. (3.20) we used Eqs. (3.19a) and (2.20b). It is seen then that, in the rate of change of $\delta\gamma$, associated with the slow motion of the beam, the first order effect of the plates is canceled by the first order toroidal corrections of the accelerating field. Therefore, the toroidal corrections (especially the 1/r dependence) of the accelerating field must be incorporated in the equations of motion. Otherwise, there is a slow drift of the beam in the radial direction. This has been

observed in several computer runs which have not included the toroidal corrections. After the toroidal corrections were included, the rate of change of $\delta\gamma$ became negligible.

c. Resonances and Multiple Frequencies in the Rebatron

In contrast to the modified betatron where the acceleration takes place continuously, in the rebatron it is a stepwise process, since the accelerating field is localized at the gap. Therefore, there is a periodicity associated with the rise of the beam energy, with period $T = 2\pi/\omega_0$ i.e., equal to the time it takes the particle to make a full turn around the torus. Let the increment per turn in γ be $\Delta\gamma$. Since the increase of γ takes place during the short time Δt that the particle crosses the accelerating gap, $\Delta t << T$, and γ is a ladder function, of the step $\Delta\gamma$ and length T. Therefore, γ can be expressed as follows:

$$\gamma(t) = \gamma_{lin}(t) + \gamma_{osc}(t), \tag{3.21a}$$

where

$$\gamma_{lin}(t) = \gamma_0 + \Delta\gamma\ (\frac{1}{2} + \frac{t}{T}),\ 0 < t < \infty, \tag{3.21b}$$

$$\gamma_{osc}(t) = \Delta\gamma\ (\frac{1}{2} - \frac{t}{T}),\qquad 0 < t < T, \tag{3.21c}$$

and $\gamma_{osc}(t + T) = \gamma_{osc}(t)$. Since the first crossing through the accelerating gap occurs at time $t = 0$, after m turns γ is equal to $\gamma = \gamma_0 + (m + 1)\ \Delta\gamma$, where γ_0 is the initial value of γ.

Since $\gamma_{osc}(t)$ is a periodic function, it can be Fourier analyzed, i.e.,

$$\gamma_{osc}(t) = \frac{\Delta\gamma}{\pi} \sum_{n=1}^{\infty} \frac{1}{n} \sin(n\omega_0 t) \ . \qquad (3.22)$$

As γ increases, the stage is reached where $|\Omega_{\theta 0}/\gamma| << \omega_w$ and the torsatron field is no longer effective and can be dropped from the equations of motion. Then, Eq. (3.5) reduces to the relation

$$\ddot{u} + i \frac{\Omega_{\theta 0}}{\gamma} \dot{u} + \frac{1}{2} \omega_0^2 \ u = \frac{c^2}{\gamma r_0} \left(\gamma - \frac{\Omega_{z0} r_0}{c}\right) , \qquad (3.23)$$

where, for simplicity, it was set $n_0 = 1/2$, and $v_\theta \approx c$. Since the vertical magnetic field B_{z0} matches at all times the linear part of γ (cf. Eq. (3.21b)), and since eventually $|\gamma_{osc}(t)| << \gamma_{lin}(t)$, Eq. (3.23) can be written approximately as

$$\ddot{u} + i \frac{\Omega_{\theta 0}}{\gamma} \dot{u} + \frac{1}{2} \omega_0^2 u \approx \frac{c^2}{\gamma_{lin} r_0} \frac{\Delta\gamma}{\pi} \sum_{n=1}^{\infty} \frac{1}{n} \sin(n\omega_0 t) \ . \qquad (3.23)$$

This is a linear second order differential equation with characteristic frequencies equal to

$$\omega_{\pm} = \frac{1}{2} \left(\sqrt{\varepsilon^2 + 2} \pm |\varepsilon| \right) \omega_0 , \qquad (3.24a)$$

where

$$|\varepsilon| = \frac{|\Omega_{\theta 0}|}{\gamma_{lin} \omega_0} = \frac{|B_{\theta 0}|}{B_{z0}} \ . \qquad (3.24b)$$

Therefore a resonance is excited when $\omega_+ = n\omega_0$, $n = 1,2,3, \ldots$, or, in terms of $|\varepsilon|$, when

$$\frac{1}{|\varepsilon|} \equiv \frac{B_{z0}}{|B_{\theta 0}|} = \frac{2n}{2n^2 - 1} \ . \qquad (3.25)$$

A similar expression has been obtained for a periodic disturbance in the modified betatron[27]. The difference here is that the occurrence of resonances in the rebatron is an inherent propery of the device due to the localized accelerating electric field and the periodic nature of the acceleration. According to Eq. (3.9b), resonance occurs each time $\gamma \approx \gamma_n$, where

$$\gamma_n = \frac{2n}{2n^2 - 1} \frac{|\Omega_{\theta o}| r_o}{c} , \tag{3.26}$$

and $n = 1, 2, \ldots$ As it will be shown in Section IV, these resonances cause the orbits to expand and, in the worst case (i.e., when $n = 1$) the beam hits the wall of the torus.

It is apparent from Eq. (3.24a) that always $\omega_- < \omega_+$. But, as the vertical magnetic field increases, ω_+ may become a multiple of ω_-, i.e., $\omega_+ = m\omega_-$. In terms of $|\varepsilon|$ this happens when

$$\frac{1}{|\varepsilon|} = \frac{B_{zo}}{|B_{\theta o}|} = \frac{\sqrt{2m}}{m - 1} , \tag{3.27}$$

where $m = 2, 3, \ldots$ The occurence of a multiple frequency changes the orbits into triangular or square shapes depending on the value of m. According to Eq. (2.9b) a multiple frequency occurs each time $\gamma \approx \gamma_m$, where

$$\gamma_m = \frac{\sqrt{2m}}{m - 1} \frac{|\Omega_{\theta o}| r_o}{c} , \tag{3.28}$$

and $m = 2, 3, \ldots$ This has been observed in the computer runs and examples will be given in Section IV.

IV. Numerical Results and their Interpretation

The various properties of the rebatron were investigated by integrating the relativistic equations of motion for the beam centroid using Eqs. (2.1) through (2.8) for the torsatron and external toroidal magnetic fields, Eqs. (2.19) through (2.23) for the magnetic field of the plates, Eq. (2.26) for the electric field of the plates, and Eqs. (2.33) through (2.37) for the accelerating electric field. The various parameters and their values are listed in Tables I, II, and III. The self fields of the beam have not been included in the computations.

To test of the extent over which the external field index confines effectively the particle orbits, some computer runs without acceleration at $\gamma = 387$ were made in the presence of a gap on the outer plate. The vertical magnetic field was set equal to $B_{zo} = 6597$ Gauss (i.e., it matches the value of $\gamma_o = 387$). The results for various initial conditions are shown in Fig. 7. As expected, when the centroid is initially at the origin, it remains there, since γ and B_z are matched at that position. On the other hand, since the external field index depends on the position and is close to one at $x = 6$ cm, $z = 0$ (cf. Fig. 5a), when the particle is placed initially there, it moves in a radial outward direction (cf. Eq. (3.14)) and eventually strikes the wall. Therefore, for the parameters chosen, the particle is successfully confined inside the torus up to distances of 5 cm from the minor axis.

In order to test the focusing effect of the torsatron magnetic field at the initial stage of the acceleration a set of runs was made without a gap on the outer plate so that $n_o\pi - 0.18$. The results are shown in Fig. 8. The initial vertical magnetic fields are: a) $B_{zo} = 341$ Gauss (it matches $\gamma_o = 20$) , in Fig. 8a, b) $B_{zo} = 3.41$ kG (it matches $\gamma_o = 200$) in Fig 8b, and c) $B_{zo} = 17.05$ kG (it matches $\gamma_o = 1000$) in Fig. 8c. In all three cases the rate of

change of the current in the plates was equal to $I_p = 1.79 \times 10^{11}$ Amp /sec. The linearly increasing vertical magnetic field of the plates matches the dotted lines of γ versus time in Figs. 8a', 8b' and 8c'. It is seen then that at low values of γ the torsatron field confines the orbit inside the torus even though the external field index has a negative value. On the other hand, at high values of γ the torsatron field is no longer effective in confining the particle orbit which becomes sensitive to the external field index (cf. Eqs. (3.14), (3.15)) .

Figures 9 and 10 provide the main results of this paper. They correspond to two different initial positions of the particle orbit. The various parameters for these computer runs are listed in Table IV. In both cases the outer plate had a gap so that $n_0 = 0.5$ at the minor axis. Figure 9A shows magnified the particle orbit during the initial steps of the acceleration. The dotted line in Fig. 9A' shows the value of γ versus time which matches the linearly increasing vertical magnetic field in the plates. In both runs, a value of γ in excess of 1850 was reached within a time of 10 usec, or within 500 revolutions. In both runs there is no appreciable drift of the particle orbits. As stated in Section III b, this is due to the fact that the rate of change of the mismatch $\delta\gamma$ has a second order dependence on the displacement and therefore, if $\delta\gamma$ is initially zero, it remains very small during the acceleration. In the initial computer runs, the toroidal corrections of the accelerating field were not included in the computations and a very slow inward or outward radial drift as well as an extreme sensitivity to the initial value of the vertical magnetic field and its rate of change were observed. Values of γ beyond 1000 could not be reached since the orbits would slowly drift and hit the wall of the torus. After the toroidal corrections were included in the computations, the drift disappeared as Figs. 9 and 10 indicate.

Another feature that is observed in Figs. 9 and 10 is the expansion of the orbits as time evolves. This is not a continuous expansion but it occurs rather in bursts, the most pronounced being when γ exceeds the value of 1800. As discussed in Section III c, in the rebatron there can be resonances (cf.Eq. (3.26)) which for the parameters chosen here, occur at $\gamma_1 = 1830$, $\gamma_2 = 523$, $\gamma_3 = 323$, $\gamma_4 = 236$, etc. The resonance at $\gamma = 1830$ can be seen clearly in Figs. 9f and 10j and causes eventually the orbit to hit the wall of the torus. This is the worst resonance and occurs when $|B_{\theta o}|/B_{zo} = 1/2$. The amplitude of the nth resonance is proportional to $1/n$ (cf. Eq. (3.23)), i.e., it decreases rather slowly with n. Therefore, the higher resonances are also noticeable. The second resonance may be seen in Fig. 11, which is the same as Fig. 9c, but magnified. Initially, when γ varies from 500 to 600 the orbit rapidly expands from 0.7 cm to 2.2 cm, but as γ keeps increasing from 600 to 900 the radial position of the orbit remains close to 2.5 cm, i.e., it does not vary as much. A comparison of the size of the orbits in Figs. 10b, 10c and 10d, indicates that there is a resonance close to $\gamma \approx 500$ in the second run too. The higher resonances beyond the second are clustered much closer together, their amplitudes are smaller and, therefore, they are not as noticeable individually. But they do cause an expansion of the particle orbit as indicated in Fig. 9a and in Figs. 10a and 10b. The value of the total toroidal magnetic field used in these runs was $B_{\theta o} = -15.6$ kG. A higher value of $B_{\theta o}$ would cause the first resonance to occur at a value of γ greater than 1830 (cf. Eq. (3.26)). Therefore, there is no intrinsic difficulty in the rebatron to accelerate the beam to one GeV and beyond.

Figure 9f indicates a radical change in the shape of the particle orbit as γ surpasses the value of 1800. A similar observation holds for Fig. 10j and also for Fig. 10f, where γ is in the neighborhood of 1100. As stated in Section IIIc, this is due to the fact that the characteristic frequencies become multiples of each other. For the parameters chosen here,

Eq. (3.28) predicts that multiple frequencies should occur when $\gamma_2 = 1830$, $\gamma_3 = 1121$, etc. Notice that in the first run there is no change at $\gamma = 1830$. This indicates that, in addition to the occurrence of a multiple frequency, some other conditions must be satisfied in order to change the shape of the orbit. A clear demonstration is given in the runs shown in Figs. 12a and 12b, where there is no acceleration. In both runs the initial position is $x_0 = 2$ cm, $z_0 = 0$, and the initial velocity is $v_x = v_z = 0$, $v_\theta = c$. Also, in both runs, $n_0 = 1/2$. In the run of Fig. 12a, $\gamma = 1830$ and $B_{z0} = 31.167$ kG (it matches $\gamma = 1830$), while in the run of Fig. 12b, $\gamma = 1121$ and $B_{z0} = 19.095$ kG (it matches $\gamma_0 = 1121$)

V. Conclusions

A detailed numerical and analytical investigation of the beam dynamics in the rebatron accelerator has been carried out. It has been shown that energies approaching one GeV can be achieved within 10 microseconds. Since the acceleration occurs in such a short time, the device may not be sensitive to the various inabilities and the loss to synchroton radiation should be small.

As a result of the periodic nature of the acceleration in the rebatron, it has been found that resonances can be excited which cause the orbits to expand and, in the worst case, the beam may hit the wall of the toroidal chamber. The worst resonance is the fundamental, i.e., $n = 1$, and it occurs when the vertical magnetic field becomes twice the total toroidal magnetic field. This could be a potential problem in the rebatron unless the toroidal magnetic field is sufficiently high so that the fundamental resonance is not excited. In the cases studied here, the total toroidal magnetic field was set at 15.6 KG which allowed the beam to be accelerated at a γ slightly higher than 1800 before the fundamental resonance was reached at $\gamma_1 = 1830$. From the computer runs, it has been concluded

that the higher resonances do cause the orbits to expand but they are not as detrimental as the fundamental resonance is.

To keep the inductive voltage managable, the vertical plates which generate the vertical magnetic field should have a low inductance. As an example, for the parameters in table II, the inductance L_p of the plates is approximately[28] 2.5 μH. A vertical magnetic field B_{zo} = 17 kG is required to reach a γ of 1000, while the plates generate at the minor axis 17.58 Gauss per kA. Therefore, the current in each plate required to generate 17 kG is I_p = 967 kA. Suppose that the acceleration time Δt = 10 μsec. Then the rate of change of the current in the plates is $\dot{I}_p = 0.967 \times 10^{11}$ Amp/sec and the inductive voltage is V_p = 242 kV, which is fairly high.

The simple analytical model of Section III, provided quite reliable results with regard to the confinement of the beam by the torsatron magnetic field. The predictions of the model are in good agreement with the numerical results. It has been shown that, at the initial stage of the acceleration, the torsatron field provides excellent confinement of the beam, and the beam equilibrium position was quite insensitive to the mismatch $\delta\gamma/\gamma$ and to the external field index n_o, as long as $\omega_w << |\Omega_{\theta o}/\gamma|$. As the beam energy increases, the stage is reached, where $\omega_w >> |\Omega_{\theta o}/\gamma|$. The torsatron field is no longer effective and the beam equilibrium position becomes sensitive to both the mismatch $\delta\gamma/\gamma$ and the external field index n_o. As mentioned in Section III b, the sensitivity in n_o may prove beneficial in providing a means for extracting the beam. (cf. Figs. 8b and 8c).

Another interesting feature of the acceleration in the rebatron is the absence of any drift of the beam when the vertical magnetic field is matched to the beam energy. As explained in Section III b, this is due to the fact that, the first order toroidal correction of the accelerating field cancels

out the first order correction of the electric field from the plates. Therefore, if the mismatch is initially zero, it will remain very small during the acceleration, and there is no drift. This has been verified in several computer runs.

In the analytical and numerical results presented in this paper, the self fields of the beam have not been included. Their effect on the beam dynamics and the acceleration process will be the subject of a future publication.

Table I

Parameters associated with the torsatron fields shown in Fig. 3. Only two terms were retained in the series of Eqs. (2.1) through (2.3).

Torus major radius r_o (cm)	= 100
Toroidal chamber minor radius ρ_w(cm)	= 10
Windings minor radius ρ_o (cm)	= 12
$\alpha = 2\pi/L$ (cm^{-1})	= 0.1
$\varepsilon_1 = 2\alpha\rho_o K_2'(2\alpha\rho_o)$	= -0.481
ℓ	= 2
Winding current I_o (kA)	= 140
Torsatron magnetic field B_o (kG)	= 5.6
External toroidal field B_{so}^{ext} (kG)	= 10

Table II

Parameters associated with the magnetic field of the plates shown in Figs. 4 and 5.

	Fig 4	Fig 5
Torus major radius r_o (cm)	= 100	100
Toroidal chamber minor radius ρ_w(cm)	= 10	10
Outer plate distance from minor axis a_o (cm)	= 12	12
Inner plate distance from minor axis a_i (cm)	= -12	-12
Half height of outer plate $h_o/2$ (cm)	= 24	24
Half height of outer gap $H_o/2$ (cm)	= 0	2.35
Half height of inner plate $h_i/2$ (cm)	= 24	24
Current in outer plate I_p (kA)	= 1	1
B_z at minor axis (Gauss)	= 18.45	17.58
External field index at minor axis n_o	= -0.18	0.5
Acceleration correction factor η_p	= 1.038	1.035

Table III

Parameters associatd with the accelerating field in the region of the gap shown in Fig. 6. There were a maximum of 51 terms retained in the series of Eqs. (2.33) through (2.37).

Torus major radius r_o (cm)	= 100
Toroidal chamber minor radius ρ_w (cm)	= 10
Half width of the gap d/2 (cm)	= 2
Half period of structure D/2 (cm)	= 62
Voltage V_o (volts)	= 1
Poloidal angle ϕ (radians)	= 0

Table IV

Parameters of the runs shown in Figs. 9 and 10.

Initial current in outer plate I_p (kA)			= 8.1
Initial vertical magnetic field from plates B_{zo} (Gauss)			= 142.4
Initial matching value of relativistic factor γ_m			= 8.35
Rate of change of current in plates I_p (Amp/sec)			= 1.8745×10^{11}
Accelerating voltage (MV)			= -2
Increment of γ per revolution			= 3.914
Initial relativistic factor γ			= 7
Initial positions (cm)	r=100		
	z=0	Fig. 9	
	s=0		
	r=100		
	z=1.0	Fig. 10	
	s=0		
Initial velocities	v_r=0		
	v_z=0		
	v_s=-c		

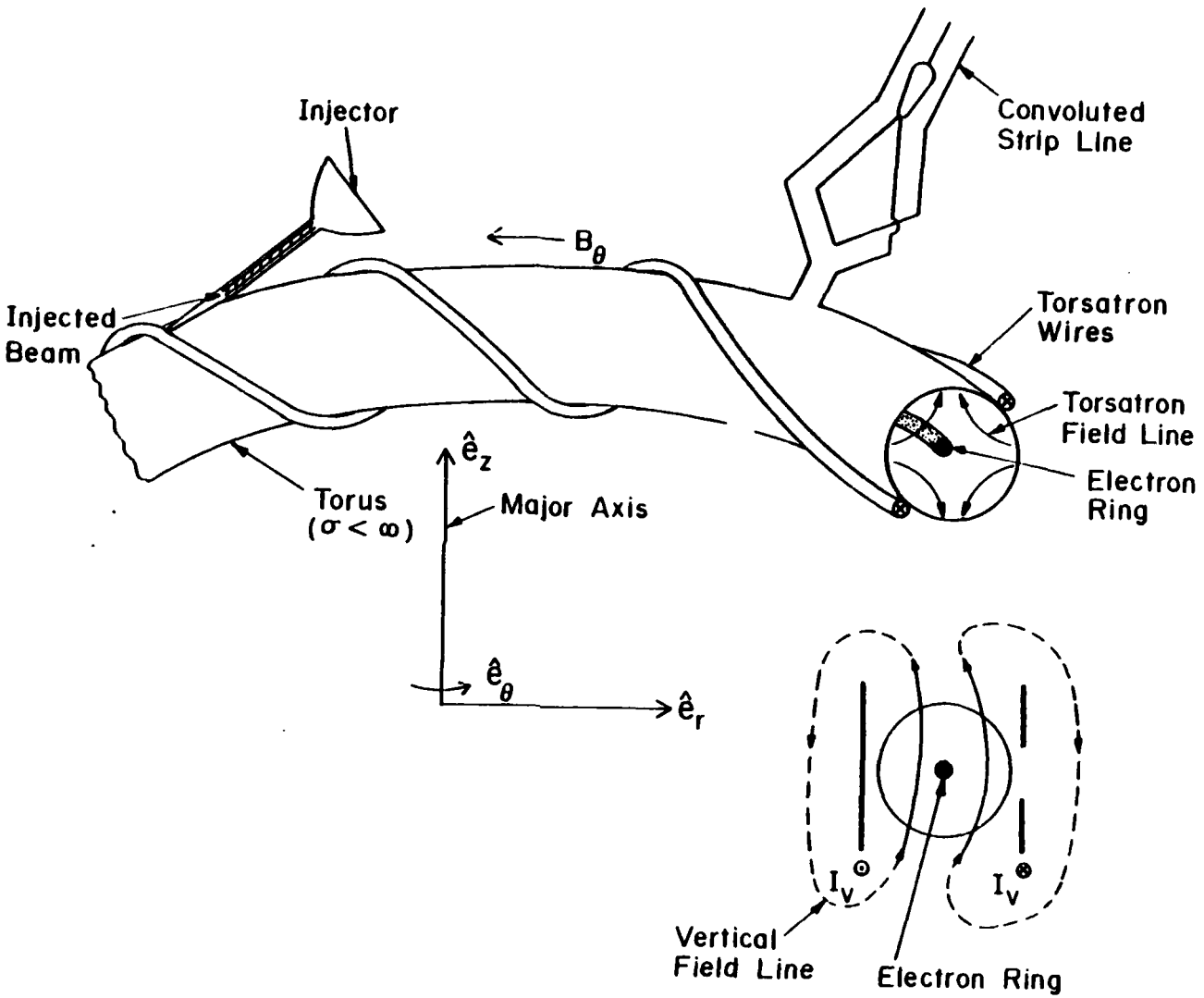

Fig. 1 — Schematic of the rebatron. The two coaxial cylindrical plates are located symmetrically around the minor axis of the torus.

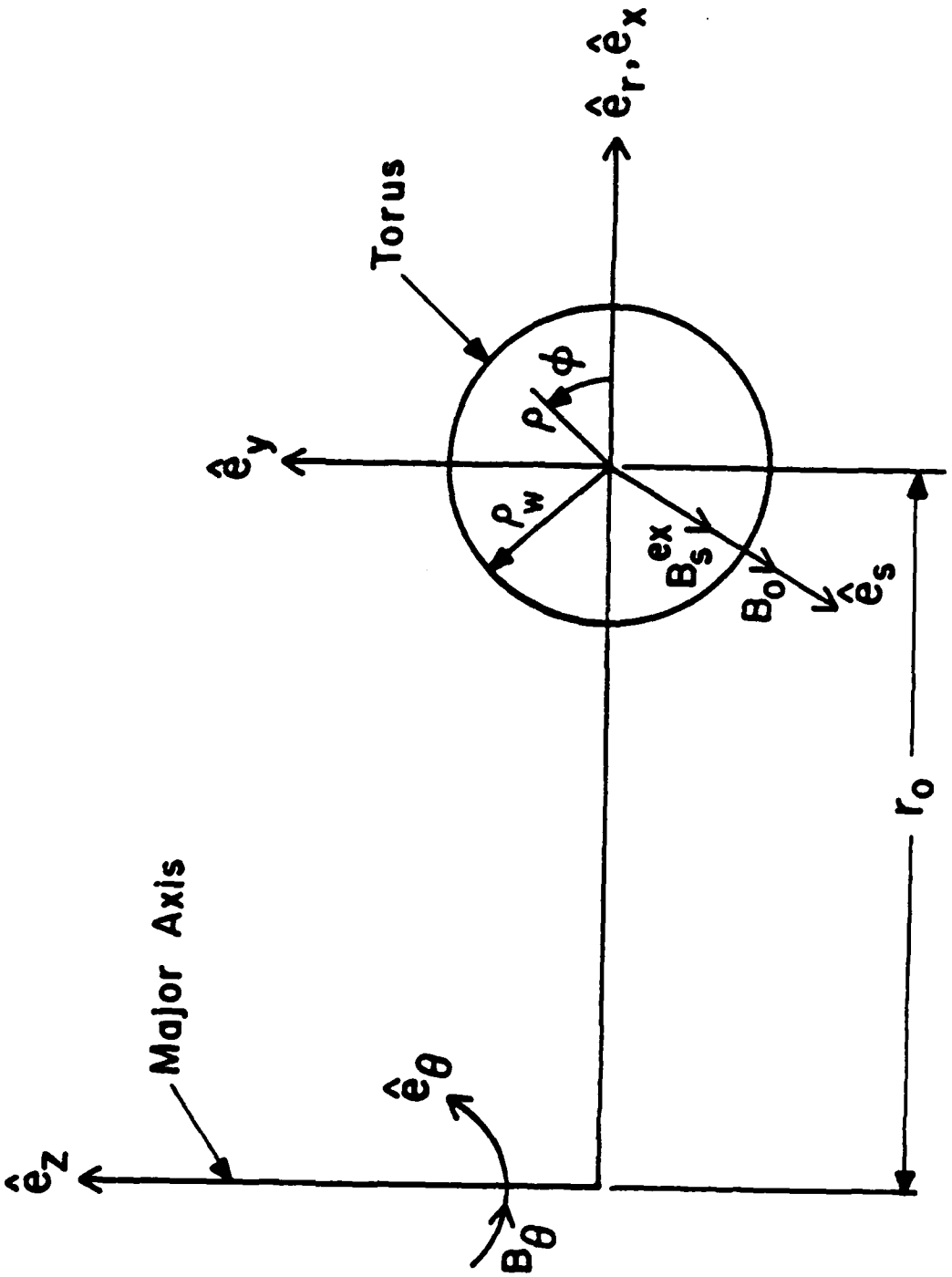

Fig. 2 — Systems of coordinates

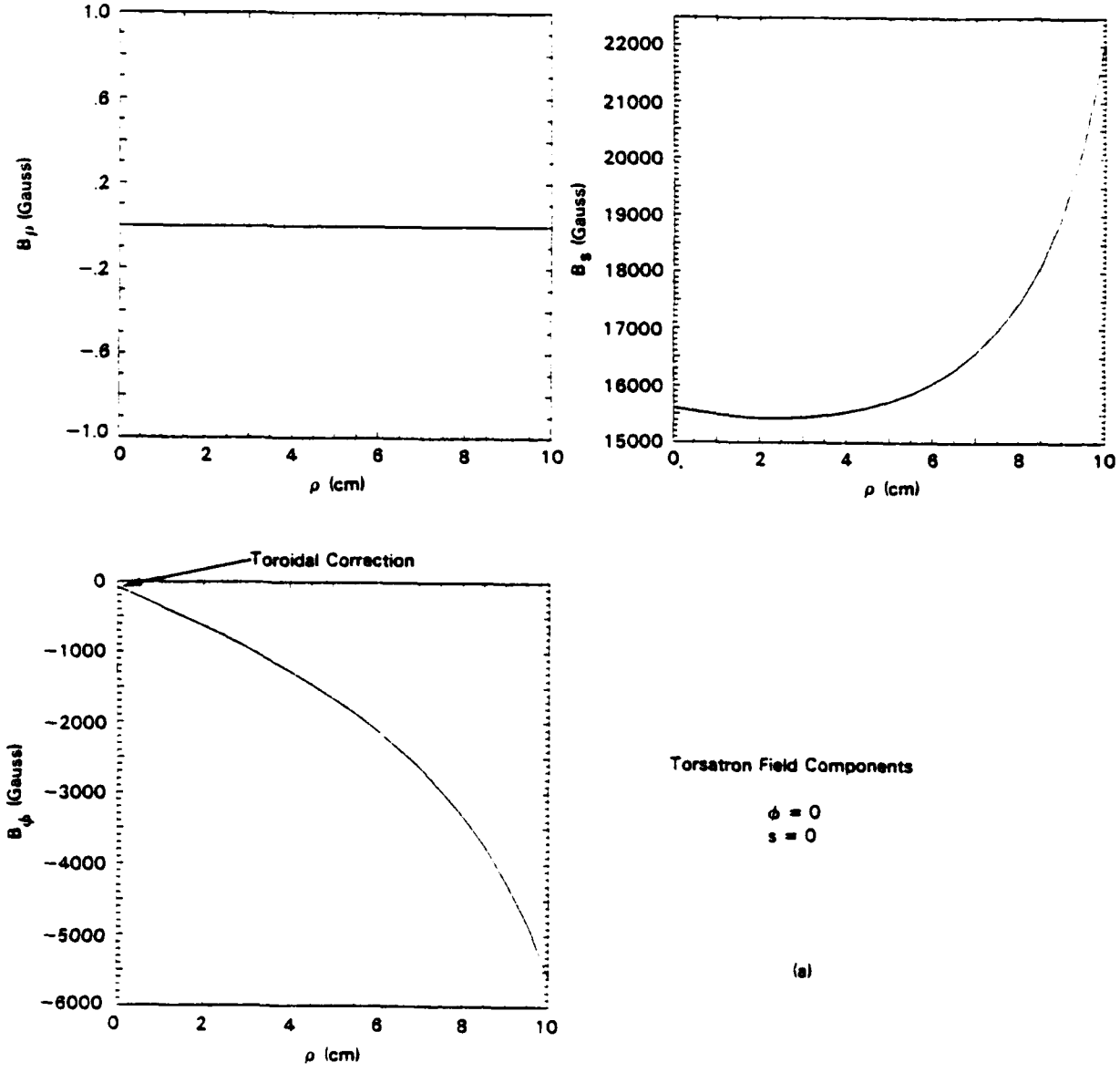

Fig. 3 — Torsatron magnetic field components (a) at $\Phi = s = o$ and (b) at $s = o$, $\Phi = \pi/2$. In addition to the torsatron field, there is a toroidal field $B_\Theta^{ext} = -10$ kG which is generated by a set of toroidal coils. (c) Magnetic field lines in (r,z) and (ρ,s) planes.

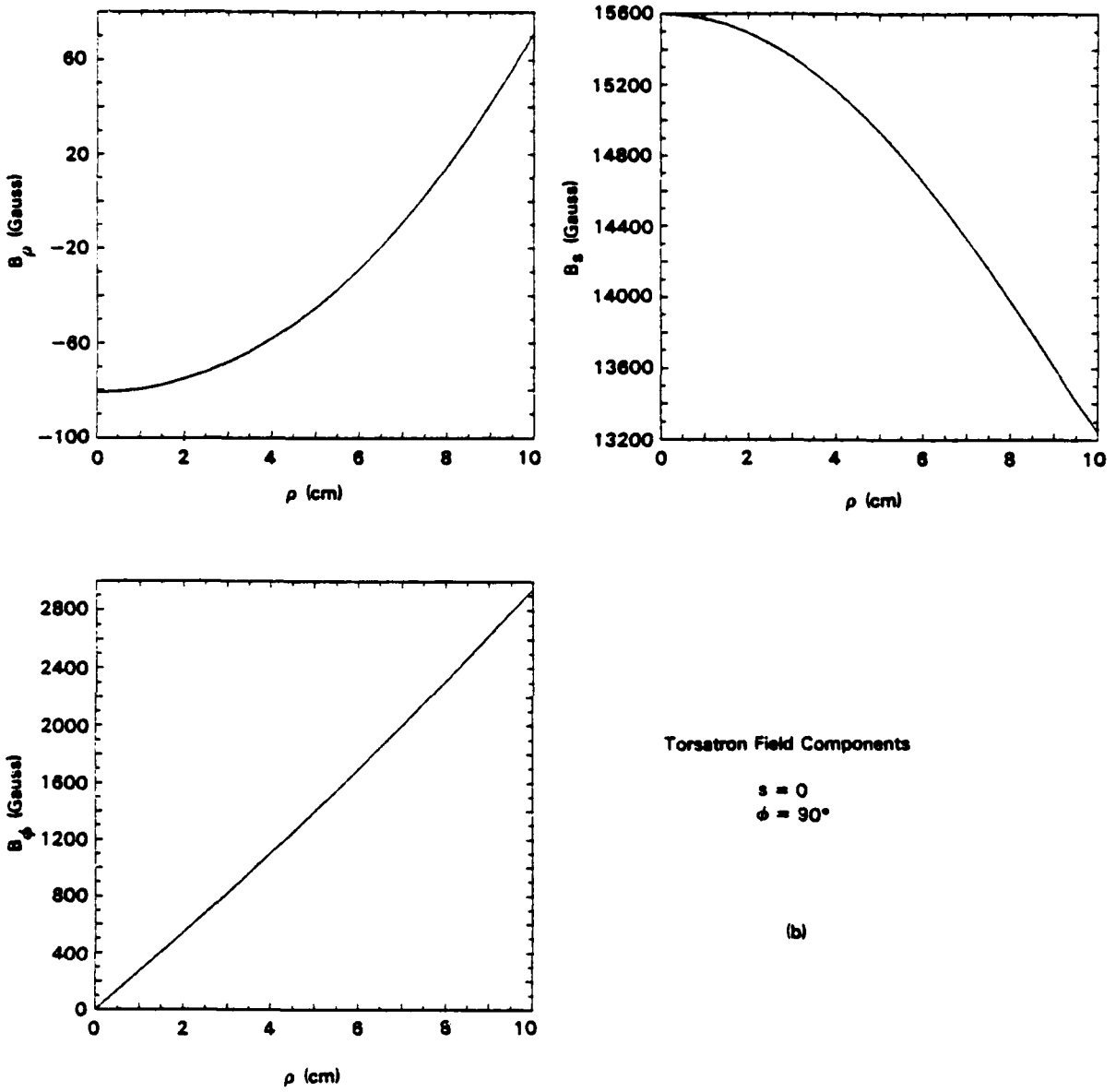

Fig. 3 (Cont'd) — Torsatron magnetic field components (a) at Φ = s = o and (b) at a toroidal field $B_\theta^{ext} = -10$ kG which is generated by a set of toroidal coils. (c) Magnetic field lines in (r,z) and (ρ,s) planes.

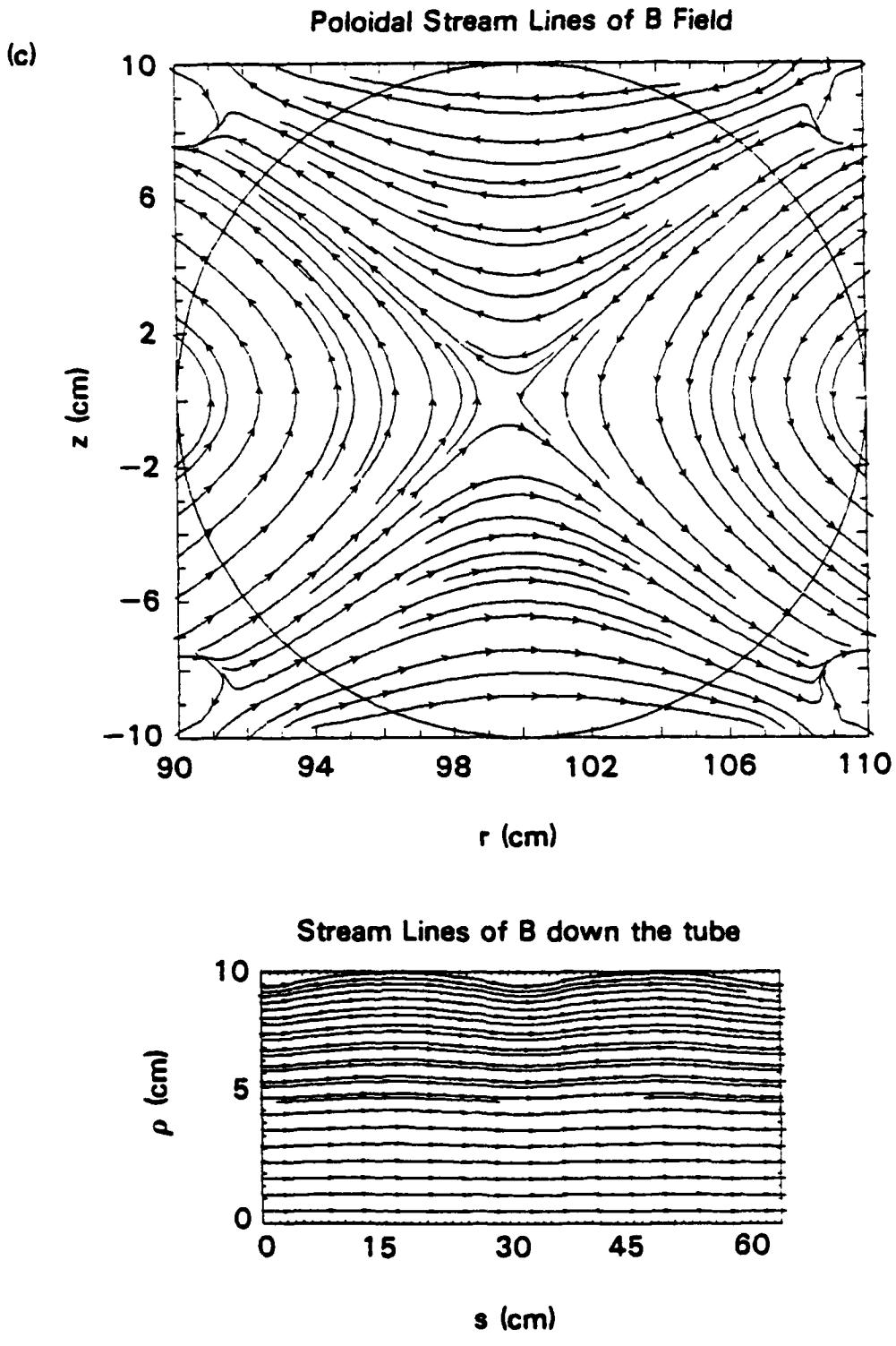

Fig. 3 (Cont'd) — Torsatron magnetic field components (a) at Φ = s = o and (b) at a toroidal field B_ϕ^{ext} = −10 kG which is generated by a set of toroidal coils. (c) Magnetic field lines in (r,z) and (ρ,s) planes.

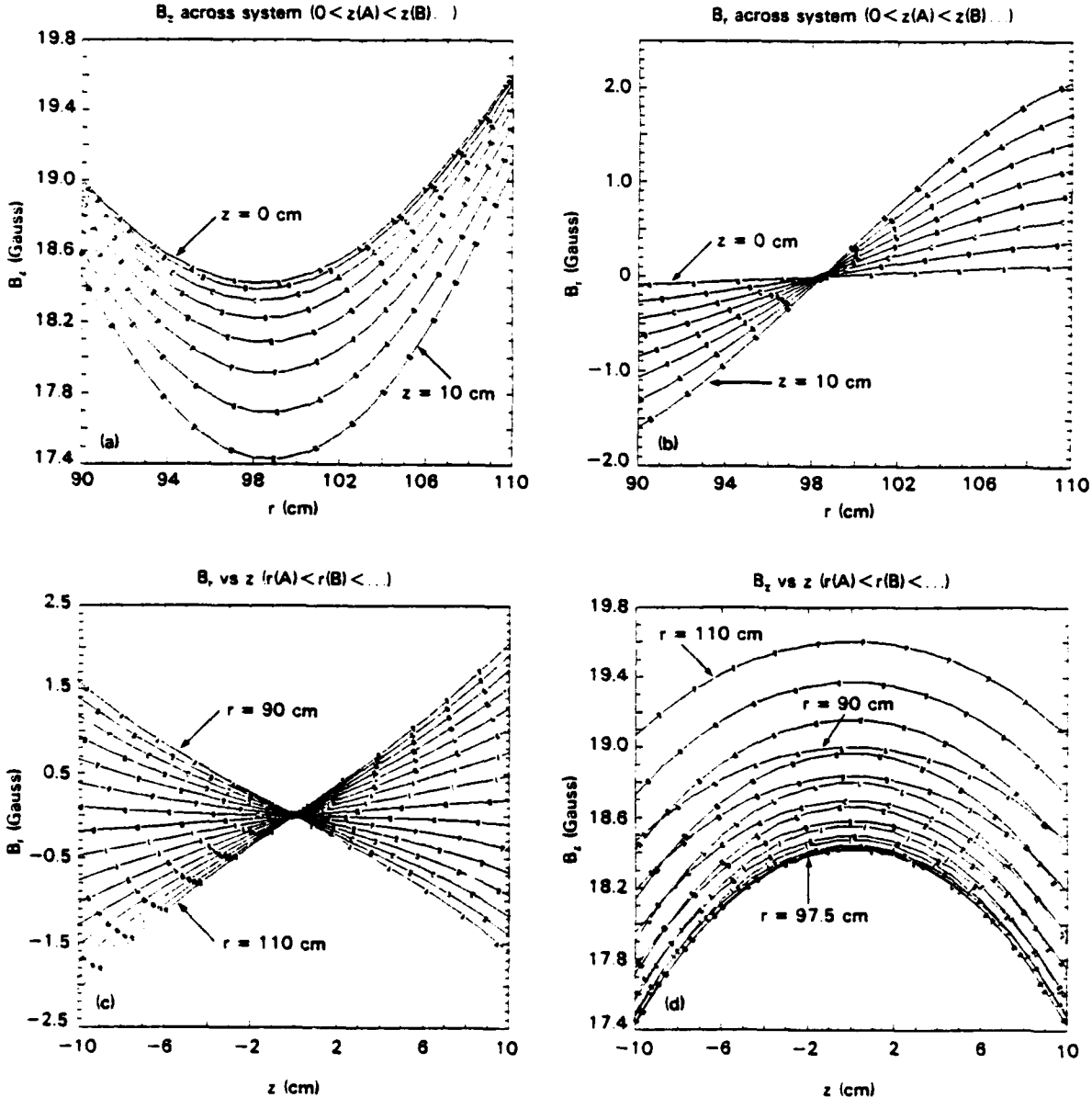

Fig. 4 — Magnetic field of plates without a gap on the outer plate, at various distances along the r-axis or the z-axis. (a) B_z versus r, (b) B_r versus r, (c) B_r versus z, and (d) B_z versus z.

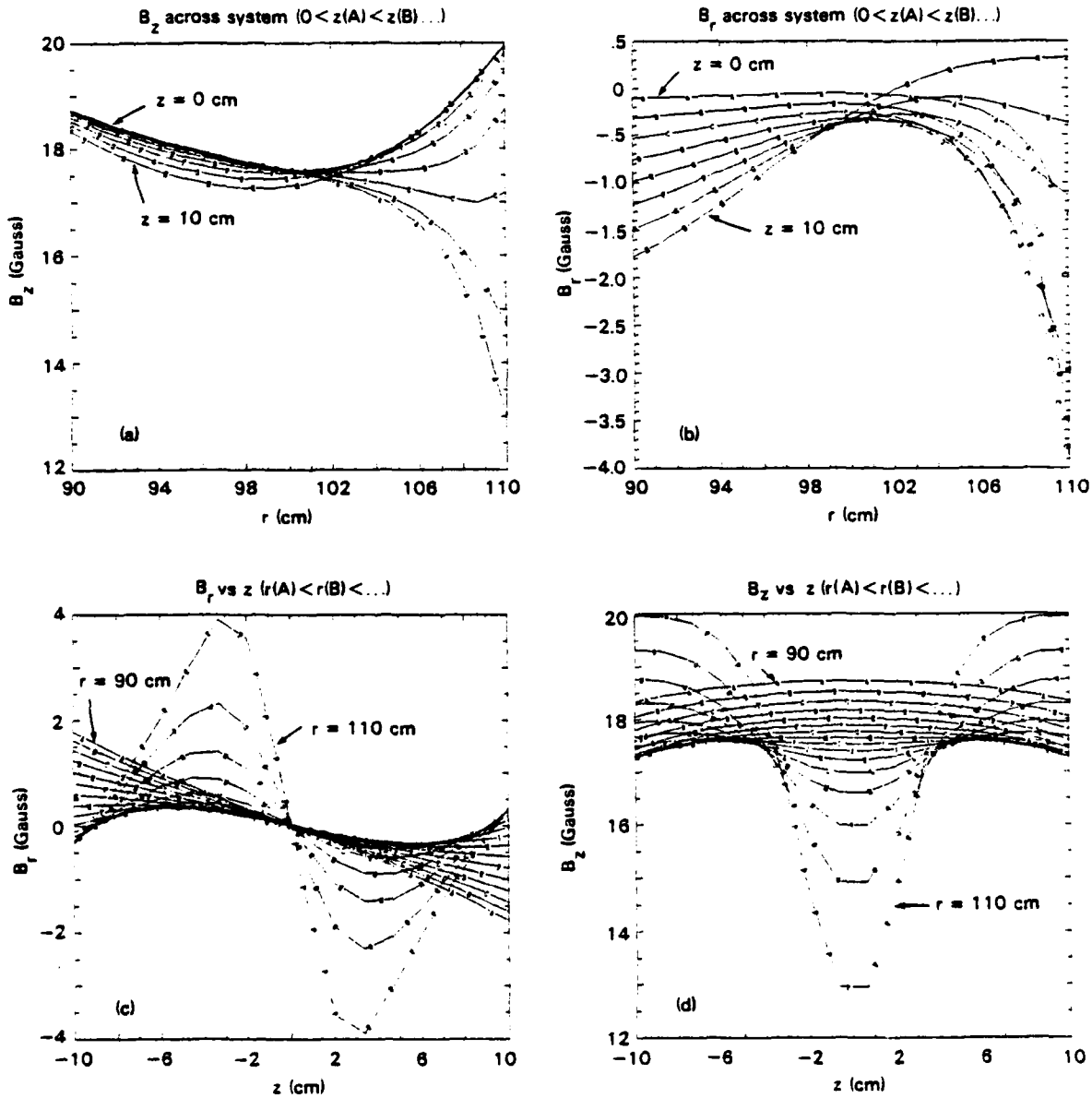

Fig. 5 — Magnetic field of plates with a gap on the outer plate, at various distances along the r-axis or the z-axis. (a) B_z versus r, (b) B_r versus r, (c) R_r versus z, and (d) B_z versus z.

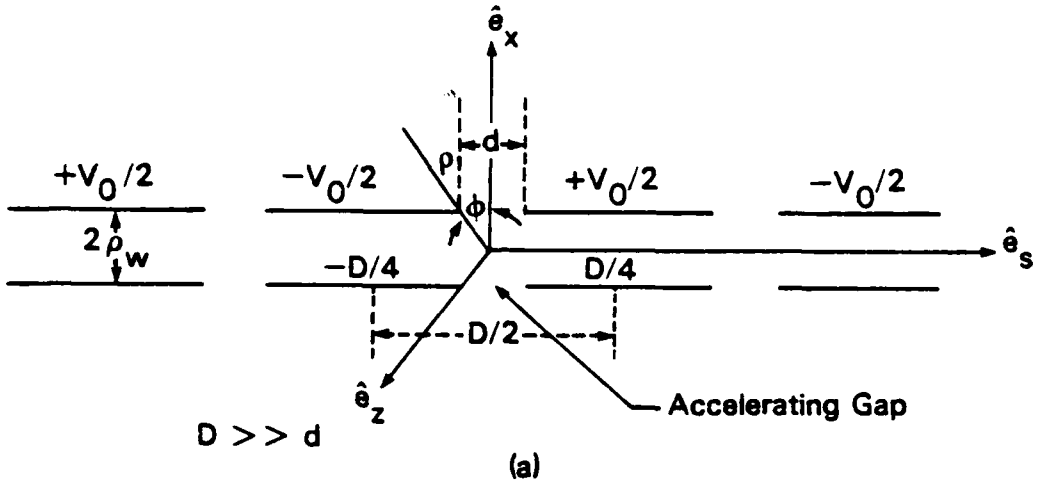

(a)

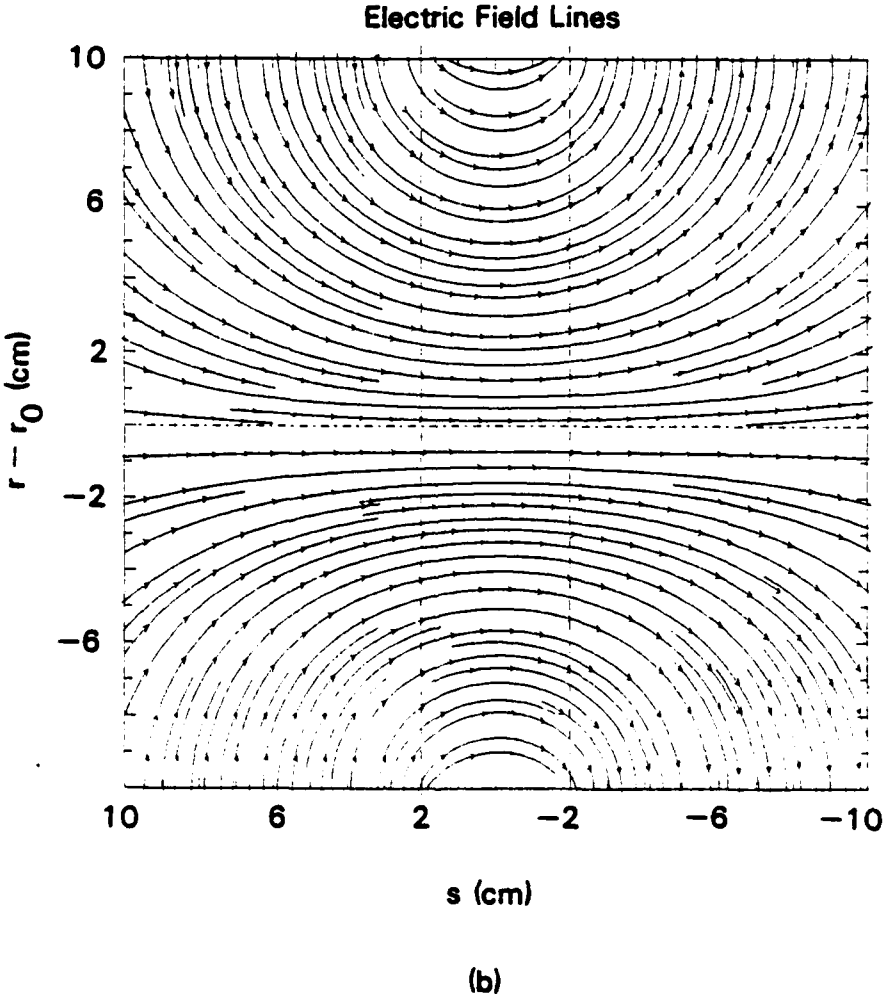

(b)

Fig. 6 — (a) Configuration, (b) field lines, (c) and (d) cylindrical components of the accelerating electric field in the region of the gap at various distances from the minor axis. The toroidal corrections have been included.

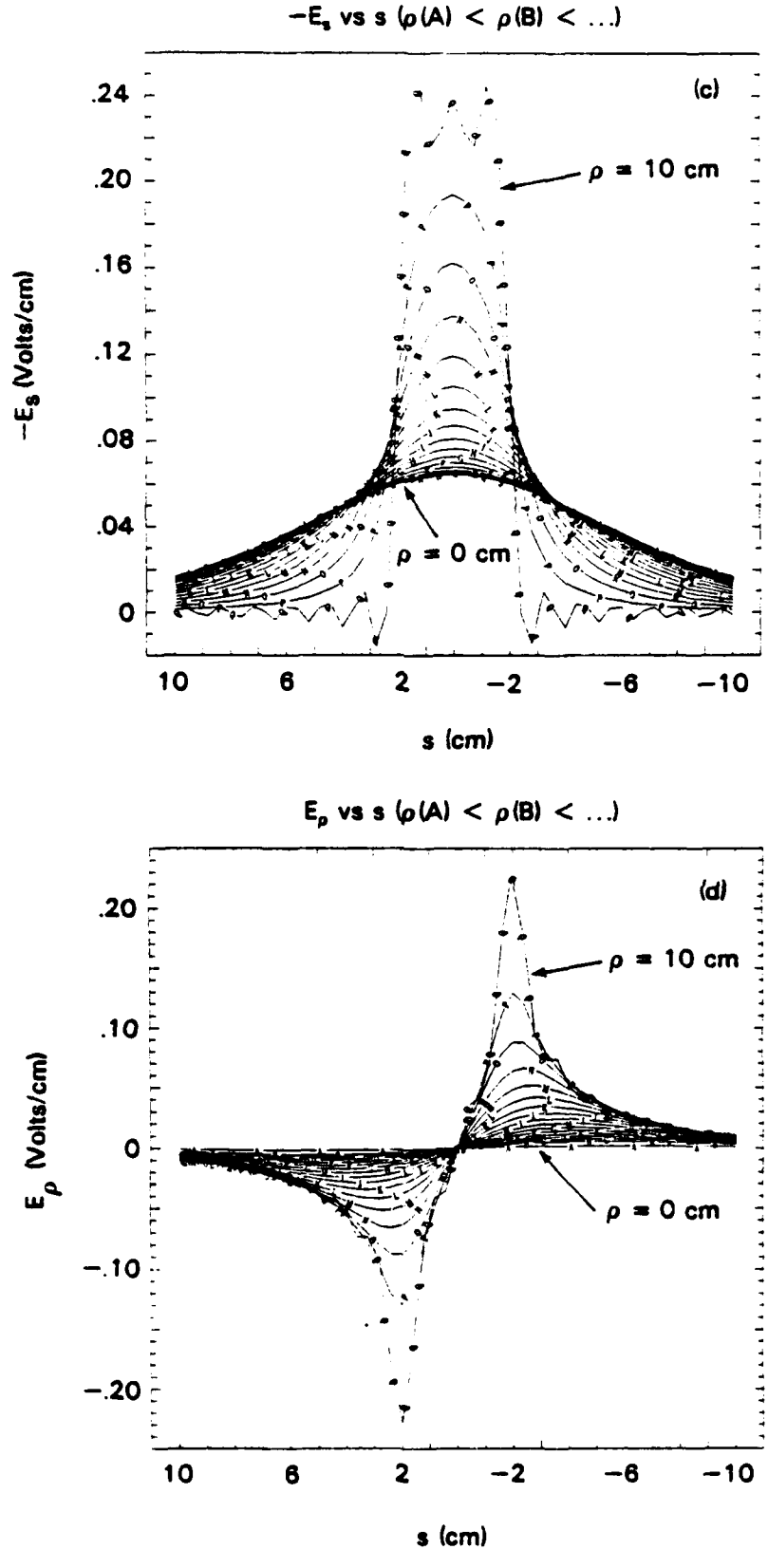

Fig. 6 (Cont'd) — (a) Configuration, (b) field lines, (c) and (d) cylindrical components of the accelerating electric field in the region of the gap at various distances from the minor axis. The toroidal corrections have been included.

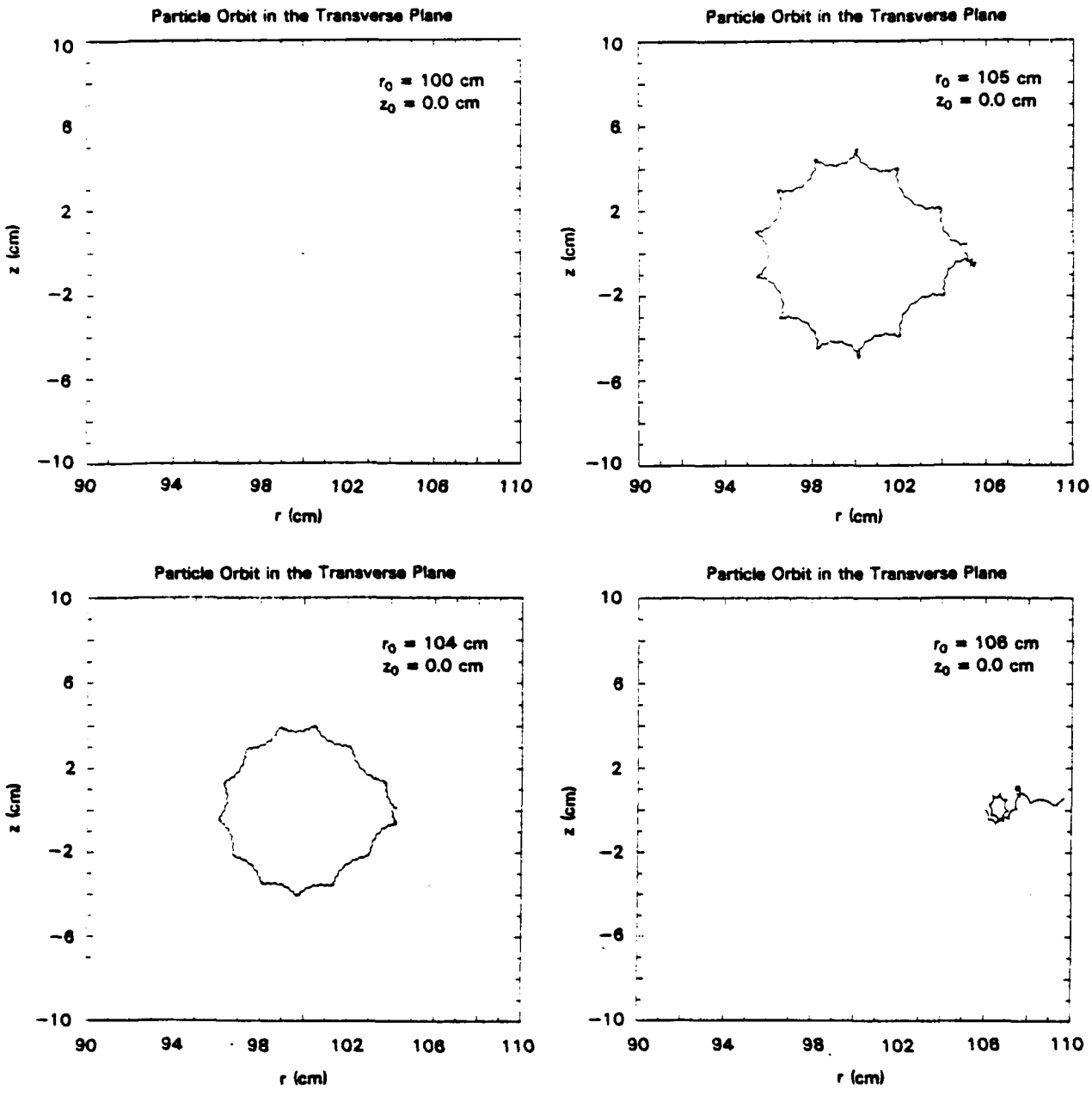

Fig. 7 — Effect of the external field index n_o of the magnetic field of the plates on the particle orbit without acceleration. The gap on the outer plate is such that n_o Π 0.5.

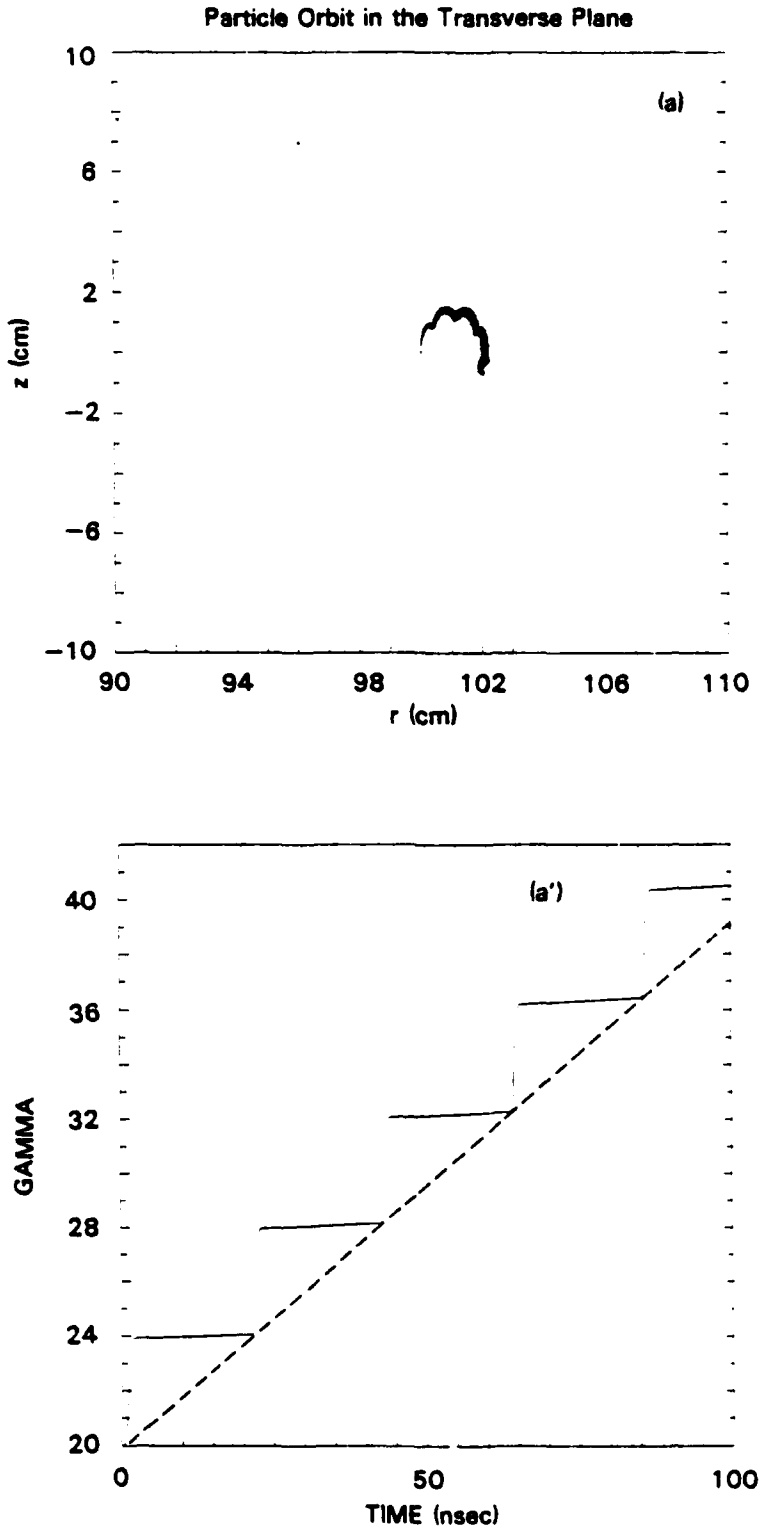

Fig. 8 — Demonstration that the particle orbit is confined by the torsatron fields only at the initial stage of the acceleration. In all cases, there is no gap on the outer plate, so that $n_o \Pi - 0.18$. Fig. (7A) is the same as Fig. (7a) but on a magnified scale.

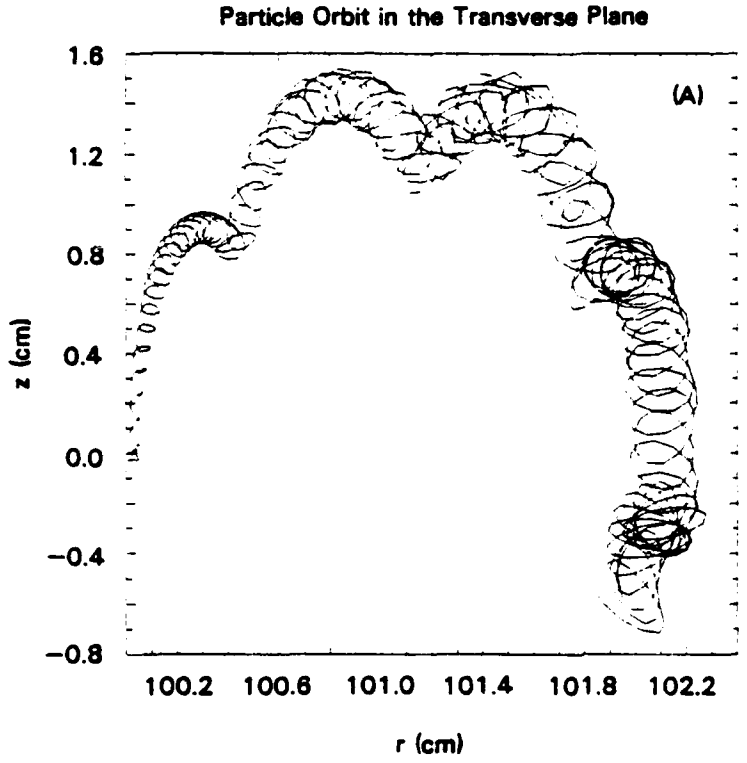

Fig. 8 (Cont'd) — Demonstration that the particle orbit is confined by the torsatron fields only at the initial stage of the acceleration. In all cases, there is no gap on the outer plate, so that $n_o \Pi - 0.18$. Fig. (7A) is the same as Fig. (7a) but on a magnified scale.

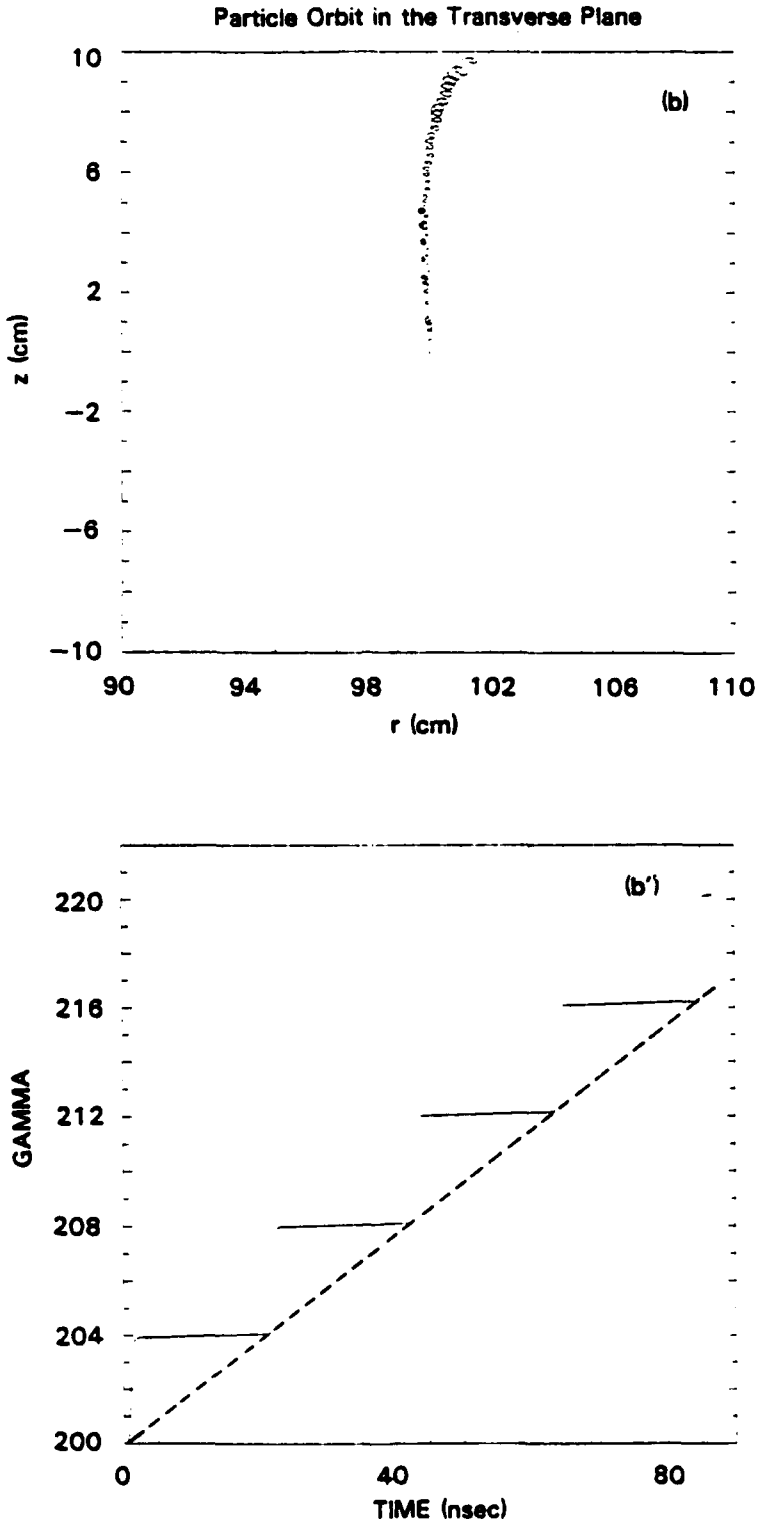

Fig. 8 (Cont'd) — Demonstration that the particle orbit is confined by the torsatron fields only at the initial stage of the acceleration. In all cases, there is no gap on the outer plate, so that $n_o \Pi - 0.18$. Fig. (7A) is the same as Fig. (7a) but on a magnified scale.

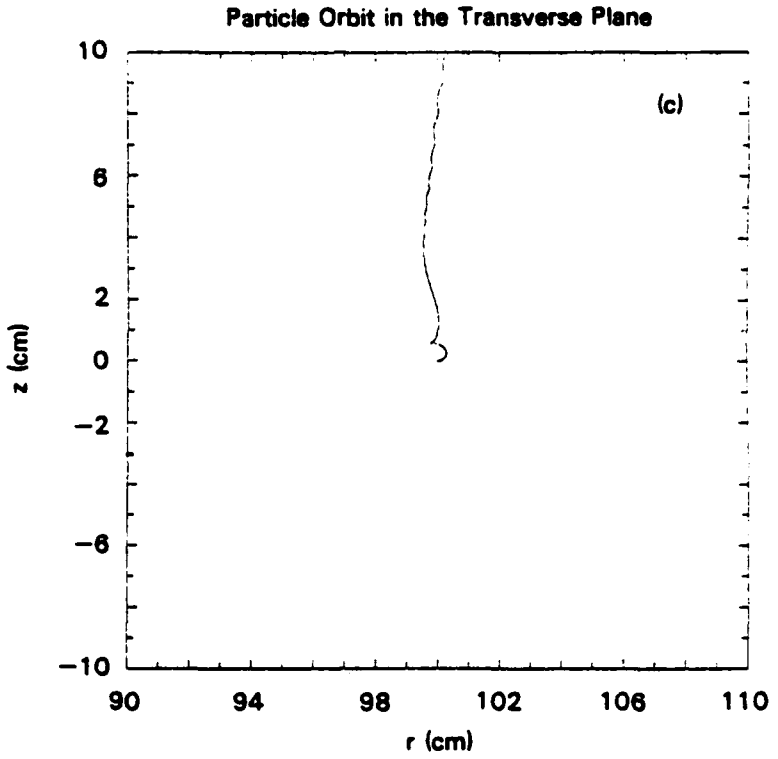

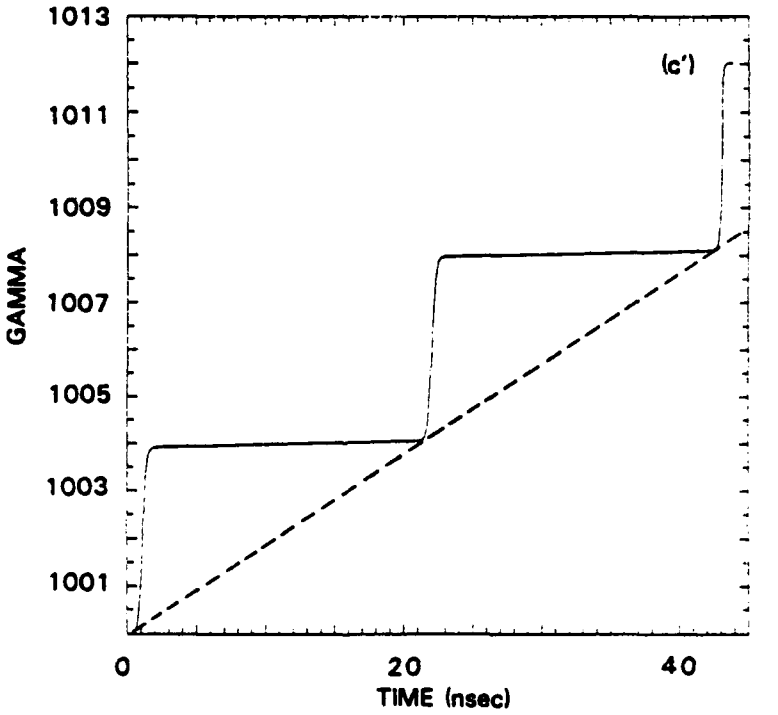

Fig. 8 (Cont'd) — Demonstration that the particle orbit is confined by the torsatron fields only at the initial stage of the acceleration. In all cases, there is no gap on the outer plate, so that $n_o \Pi - 0.18$. Fig. (7A) is the same as Fig. (7a) but on a magnified scale.

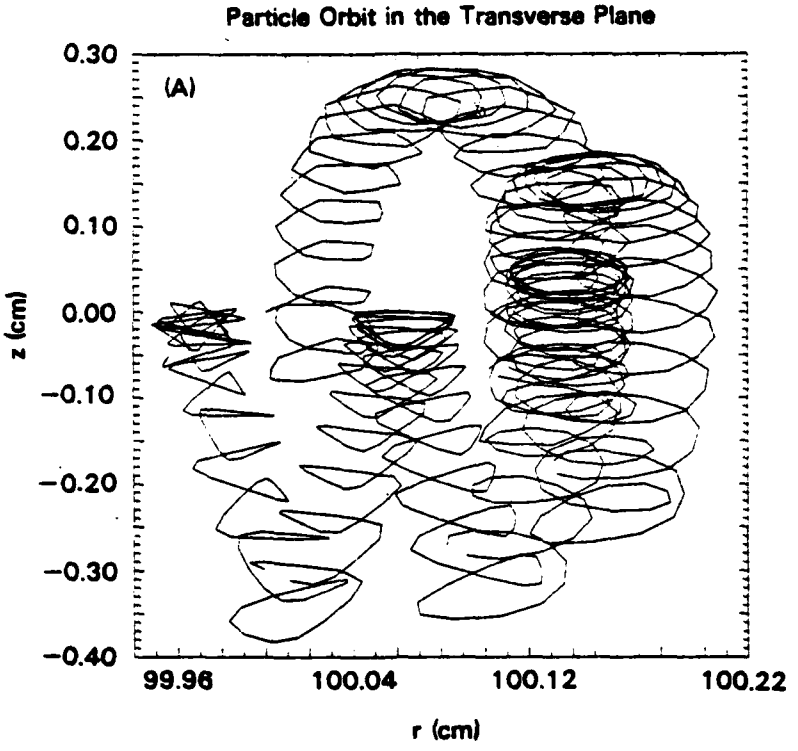

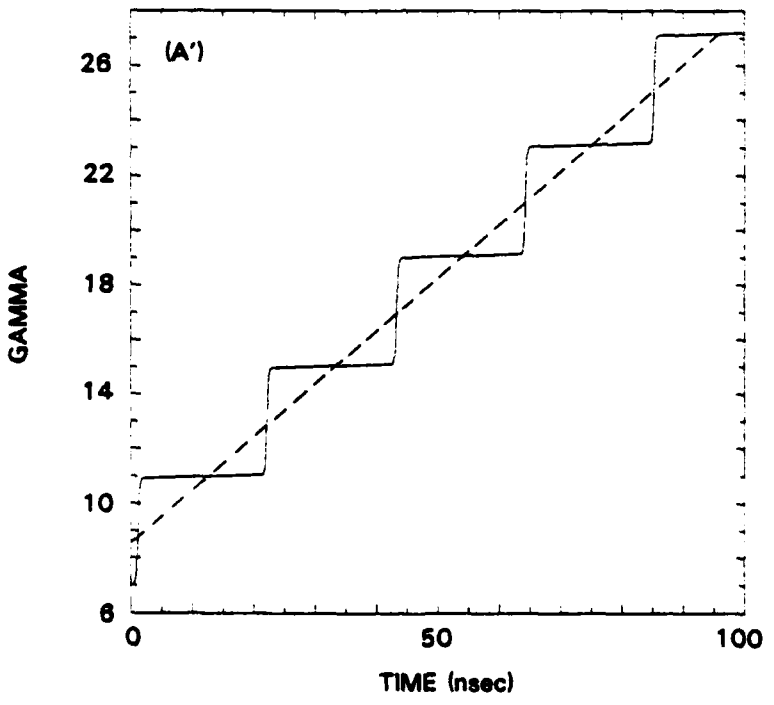

Fig. 9 — Particle orbit on the (r,z) plane (Figs. 9(a) through 9(f)) and the corresponding relativistic factor γ (Figs. 9(a') through 9(f')). The initial position of the particle is at r = 100 cm, z = 0 cm. The particle orbit and γ at the initial stage of the acceleration are shown on Figs. 9(A) and 9(A')).

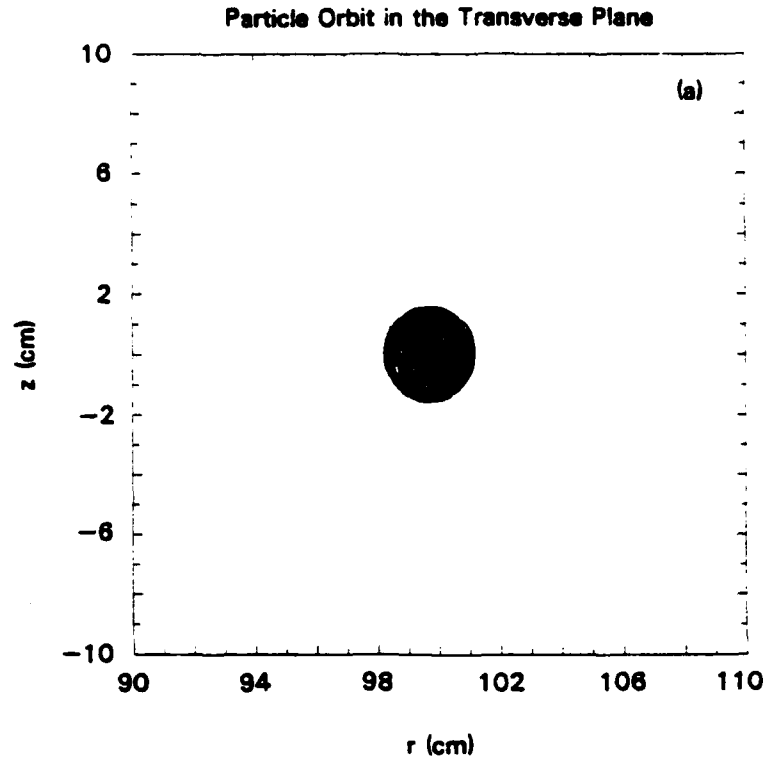

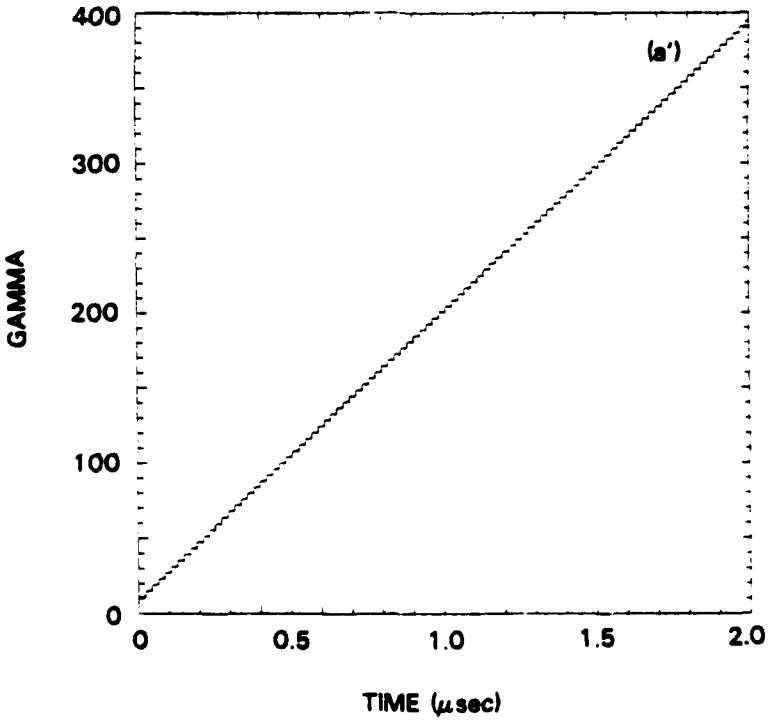

Fig. 9 (Cont'd) — Particle orbit on the (r,z) plane (Figs. 9(a) through 9(f)) and the corresponding relativistic factor γ (Figs. 9(a') through 9(f')). The initial position of the particle is at r = 100 cm, z = 0 cm. The particle orbit and γ at the initial stage of the acceleration are shown on Figs. 9(A) and 9(A')).

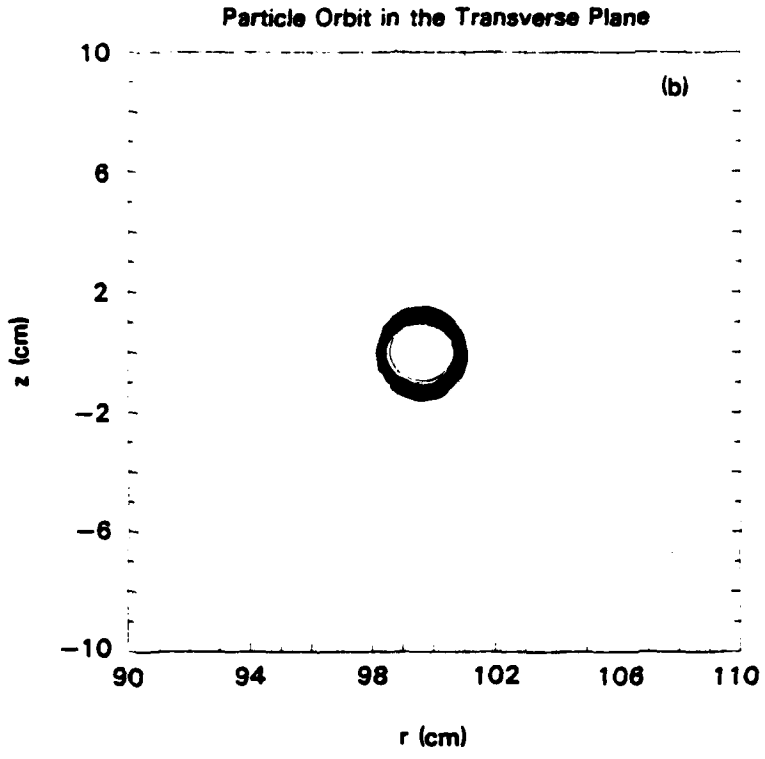

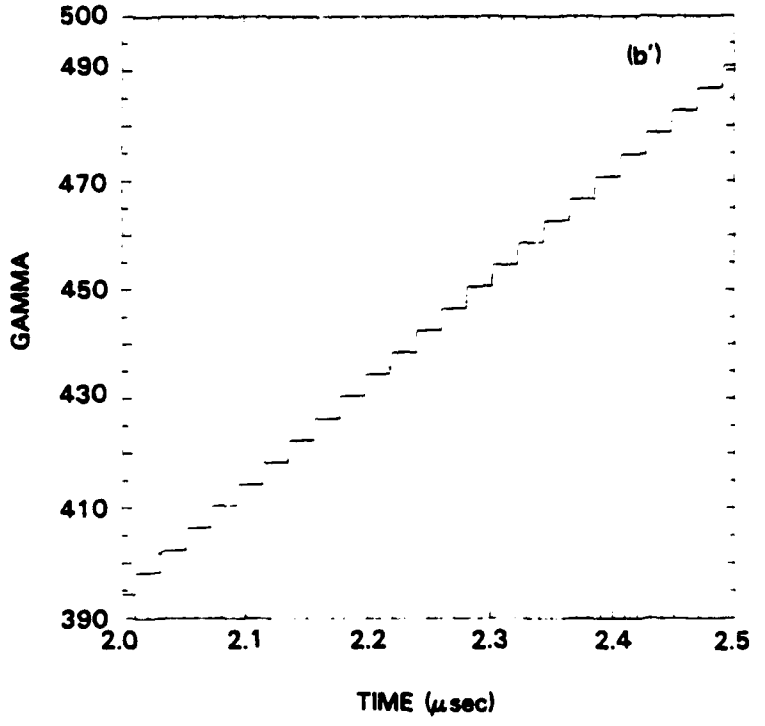

Fig. 9 (Cont'd) — Particle orbit on the (r,z) plane (Figs. 9(a) through 9(f)) and the corresponding relativistic factor γ (Figs. 9(a') through 9(f')). The initial position of the particle is at r = 100 cm, z = 0 cm. The particle orbit and γ at the initial stage of the acceleration are shown on Figs. 9(A) and 9(A')).

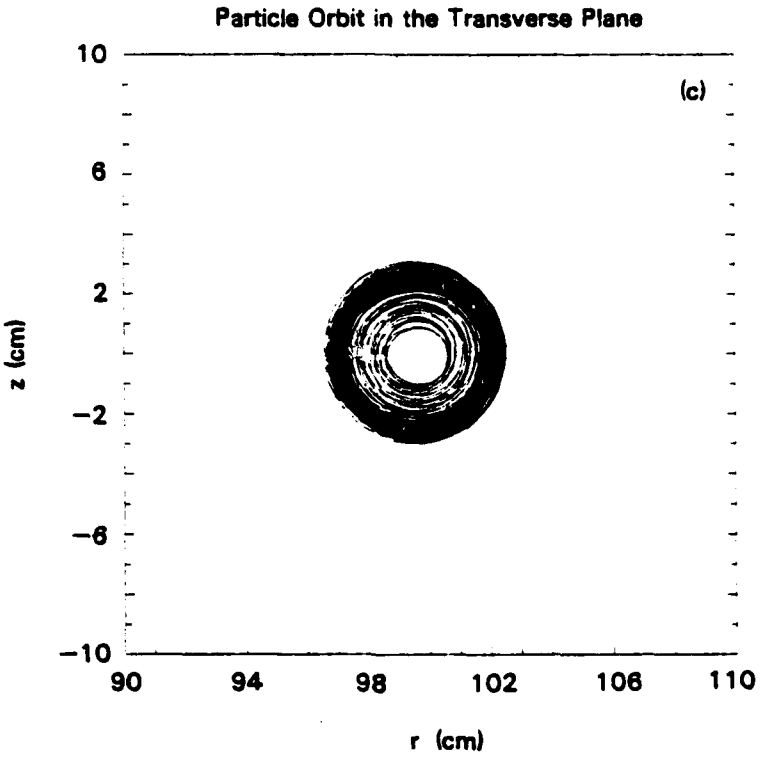

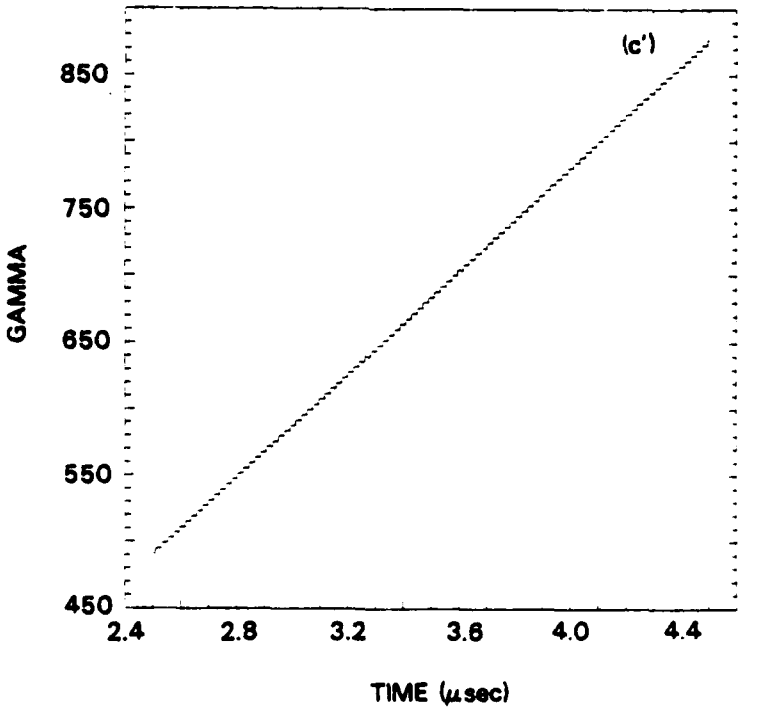

Fig. 9 (Cont'd) — Particle orbit on the (r,z) plane (Figs. 9(a) through 9(f)) and the corresponding relativistic factor γ (Figs. 9(a') through 9(f')). The initial position of the particle is at r = 100 cm, z = 0 cm. The particle orbit and γ at the initial stage of the acceleration are shown on Figs. 9(A) and 9(A')).

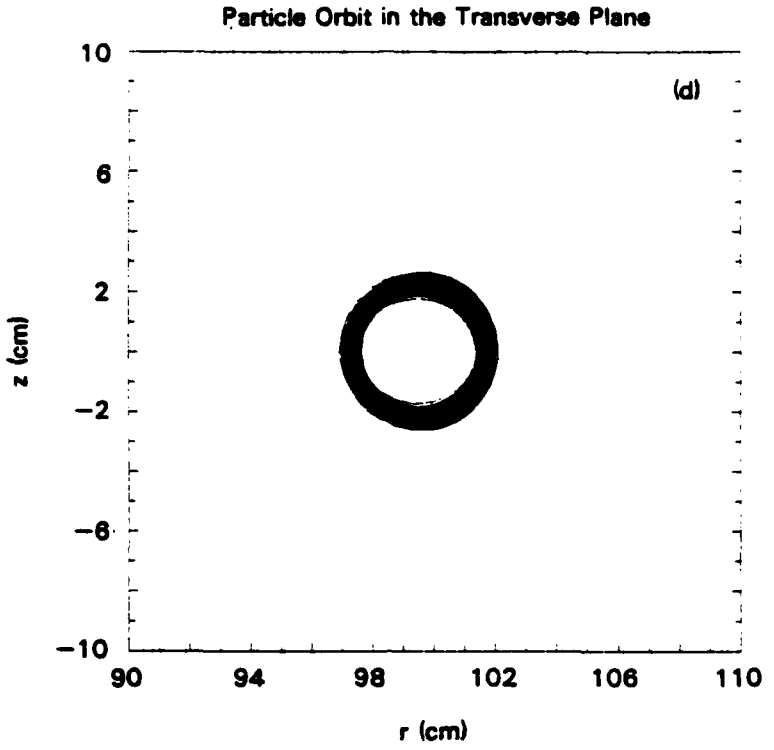

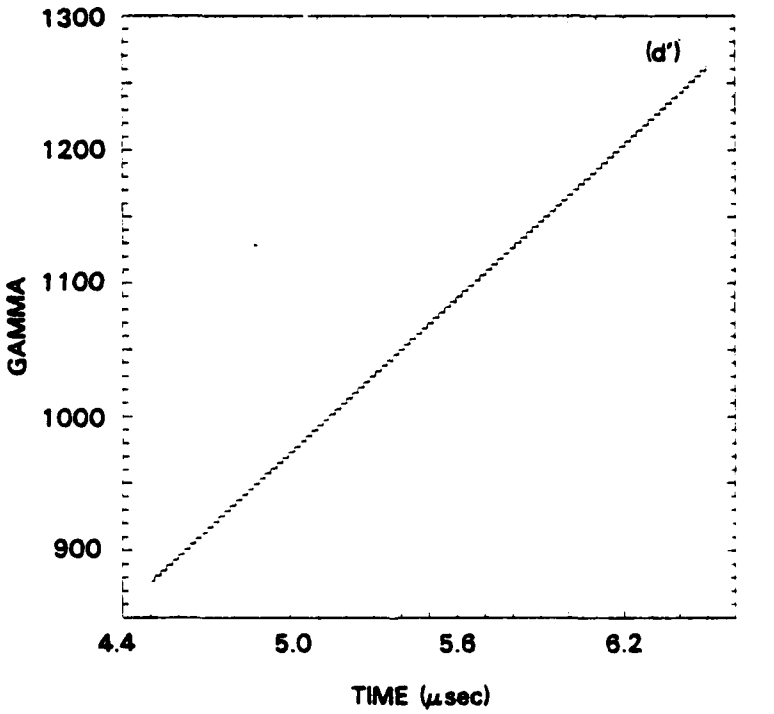

Fig. 9 (Cont'd) — Particle orbit on the (r,z) plane (Figs. 9(a) through 9(f)) and the corresponding relativistic factor γ (Figs. 9(a') through 9(f')). The initial position of the particle is at r = 100 cm, z = 0 cm. The particle orbit and γ at the initial stage of the acceleration are shown on Figs. 9(A) and 9(A')).

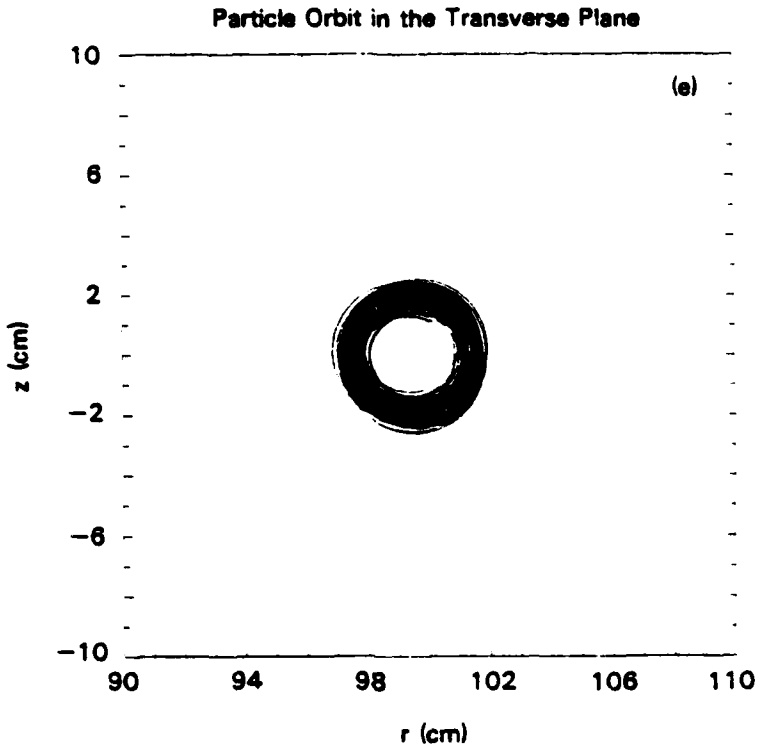

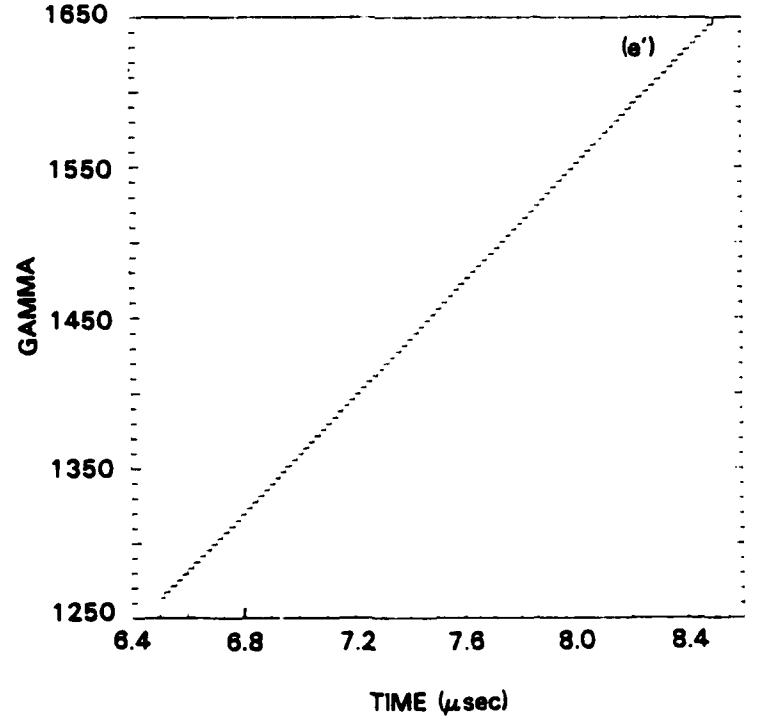

Fig. 9 (Cont'd) — Particle orbit on the (r,z) plane (Figs. 9(a) through 9(f)) and the corresponding relativistic factor γ (Figs. 9(a') through 9(f')). The initial position of the particle is at r = 100 cm, z = 0 cm. The particle orbit and γ at the initial stage of the acceleration are shown on Figs. 9(A) and 9(A')).

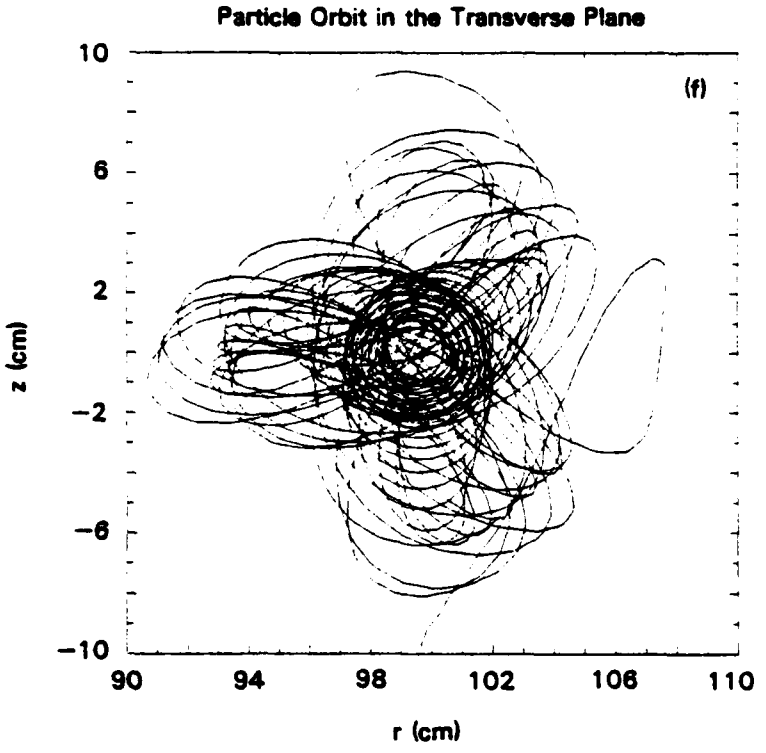

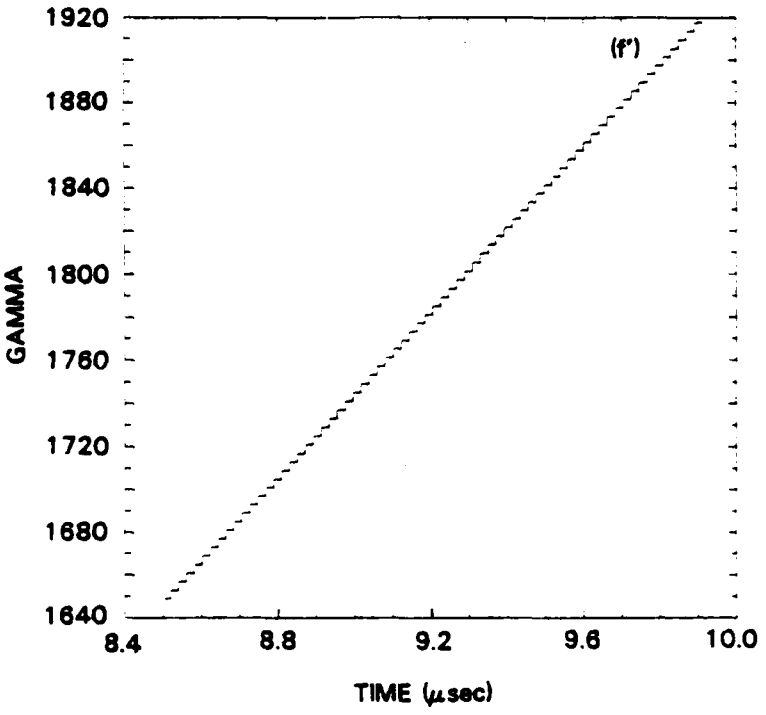

Fig. 9 (Cont'd) — Particle orbit on the (r,z) plane (Figs. 9(a) through 9(f)) and the corresponding relativistic factor γ (Figs. 9(a') through 9(f')). The initial position of the particle is at r = 100 cm, z = 0 cm. The particle orbit and γ at the initial stage of the acceleration are shown on Figs. 9(A) and 9(A')).

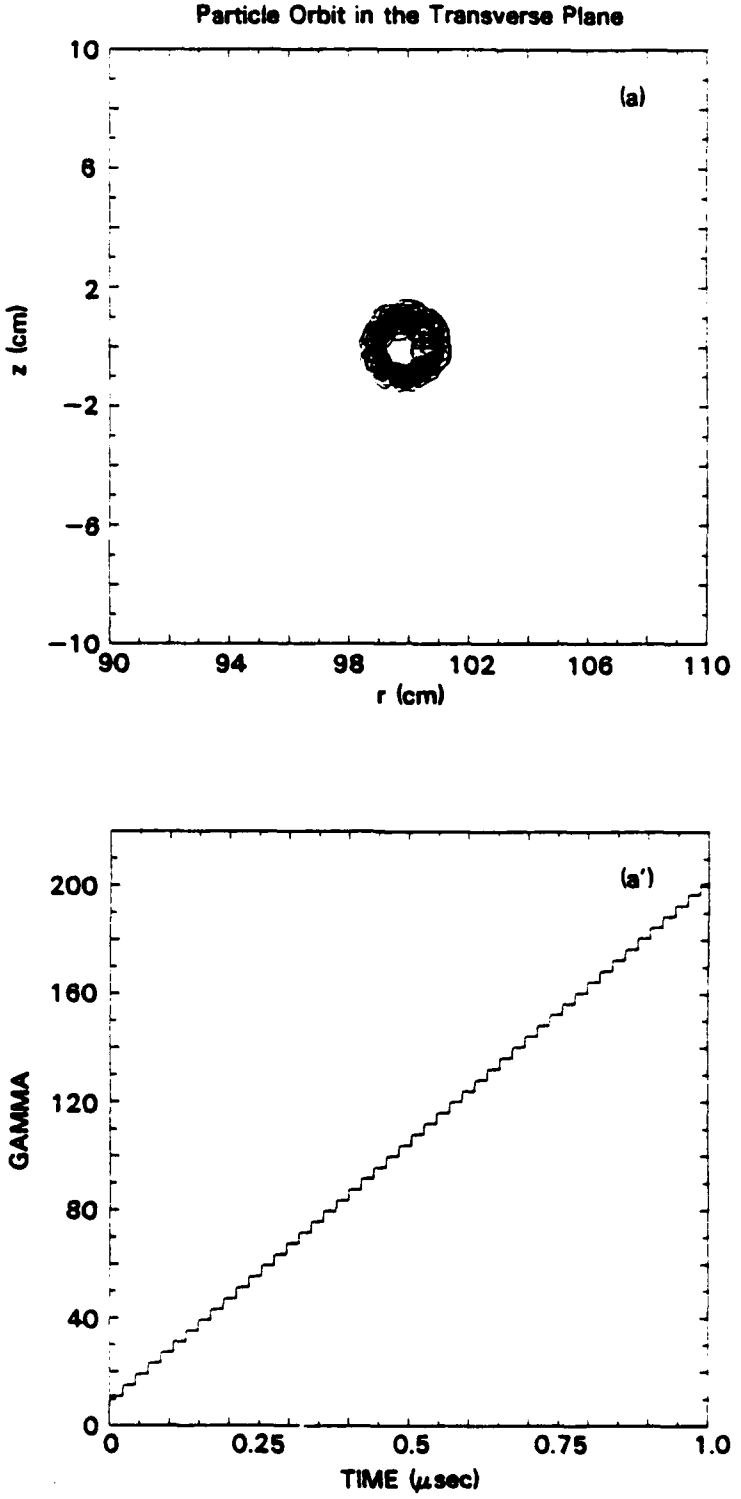

Fig. 10 — Particle orbit on the (r,z) plane (Figs. 10(a) through 10(j)) and the corresponding relativistic factor γ (Figs. 10(a') through 10(j')). The initial position of the particle is at r = 100 cm, z = 1 cm. The parameters of this run are listed in Table IV.

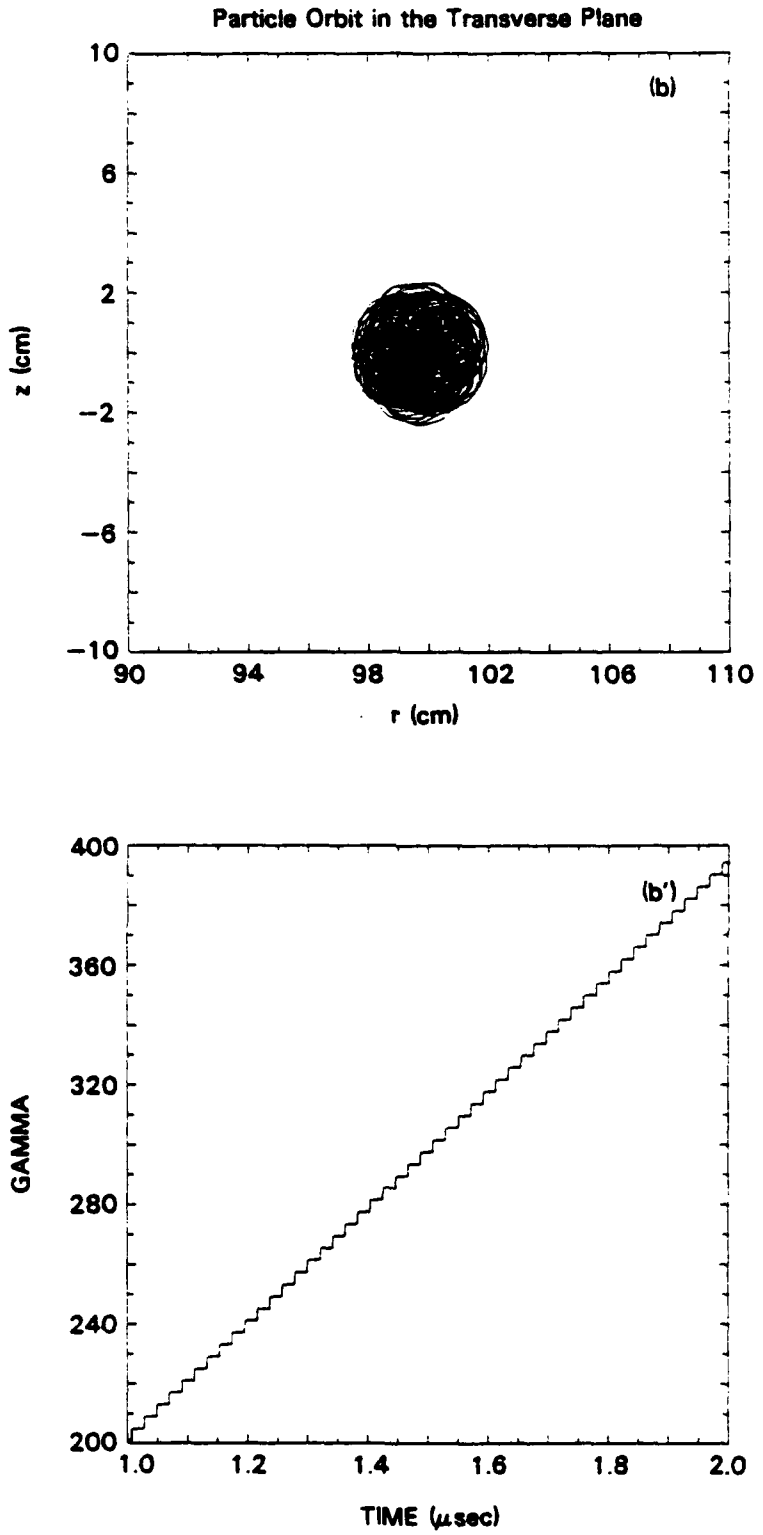

Fig. 10 (Cont'd) — Particle orbit on the (r,z) plane (Figs. 10(a) through 10(j)) and the corresponding relativistic factor γ (Figs. 10(a') through 10(j')). The initial position of the particle is at r = 100 cm, z = 1 cm. The parameters of this run are listed in Table IV.

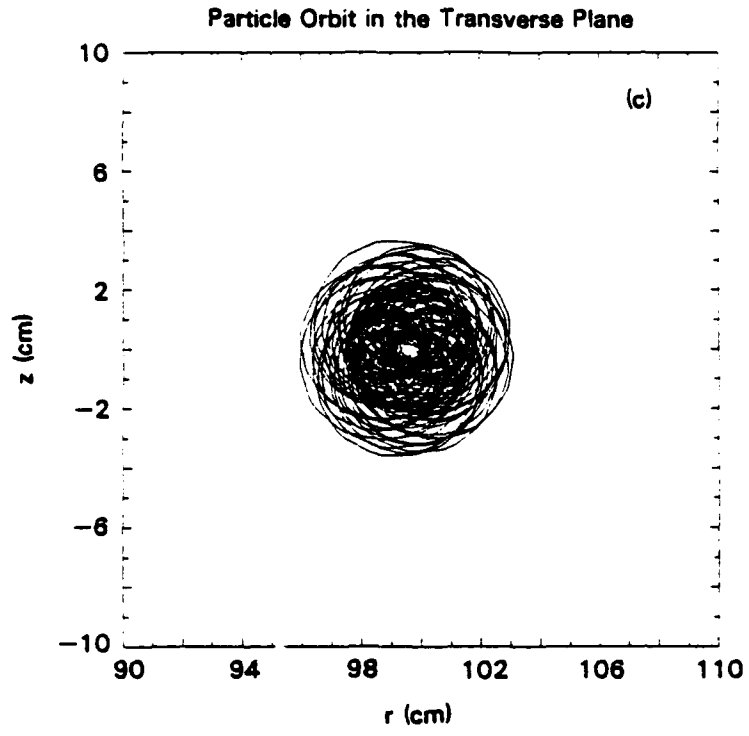

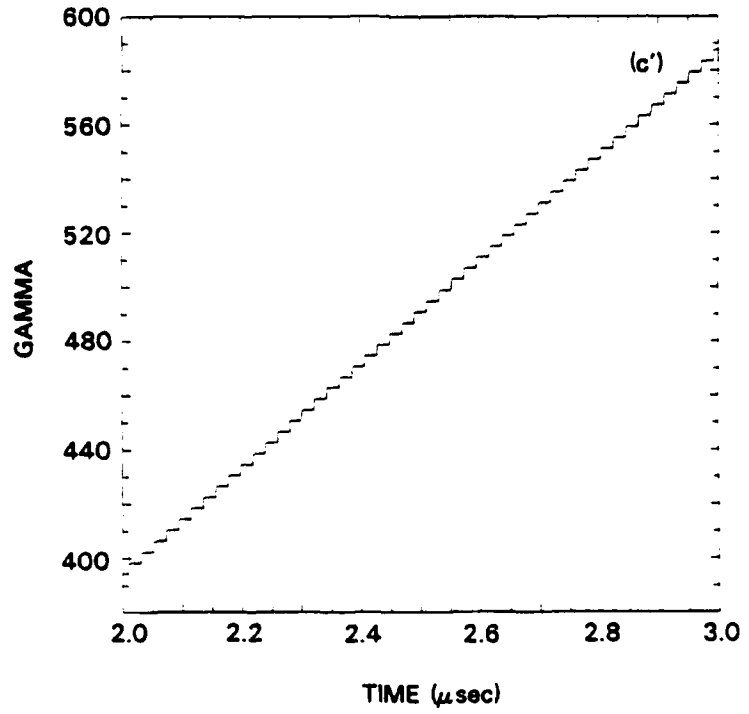

Fig. 10 (Cont'd) — Particle orbit on the (r,z) plane (Figs. 10(a) through 10(j)) and the corresponding relativistic factor γ (Figs. 10(a') through 10(j')). The initial position of the particle is at r = 100 cm, z = 1 cm. The parameters of this run are listed in Table IV.

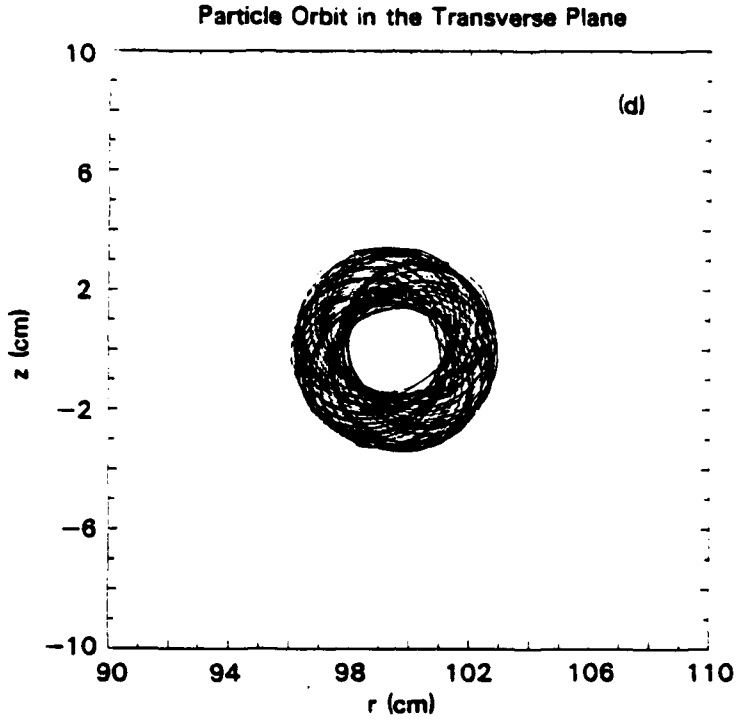

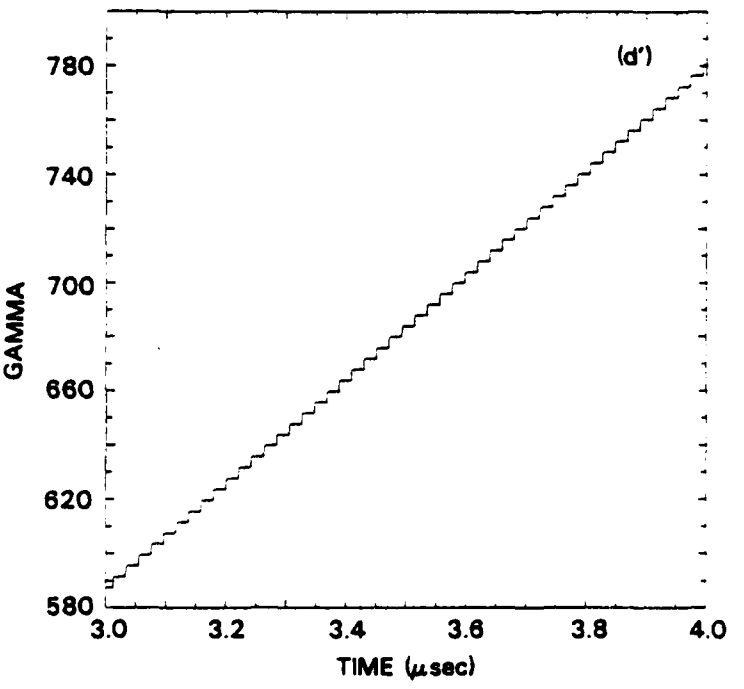

Fig. 10 (Cont'd) — Particle orbit on the (r,z) plane (Figs. 10(a) through 10(j)) and the corresponding relativistic factor γ (Figs. 10(a') through 10(j')). The initial position of the particle is at r = 100 cm, z = 1 cm. The parameters of this run are listed in Table IV.

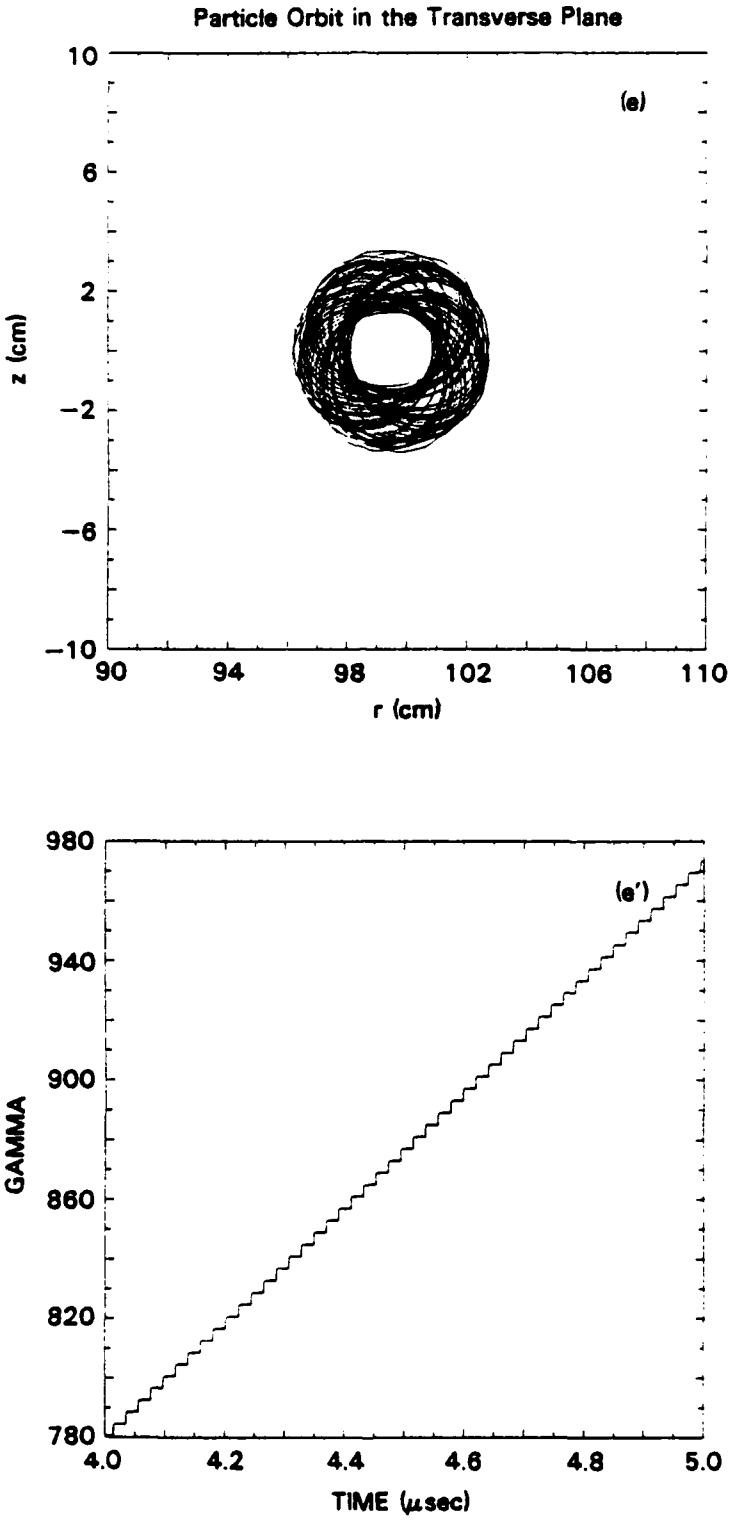

Fig. 10 (Cont'd) — Particle orbit on the (r,z) plane (Figs. 10(a) through 10(j)) and the corresponding relativistic factor γ (Figs. 10(a') through 10(j')). The initial position of the particle is at r = 100 cm, z = 1 cm. The parameters of this run are listed in Table IV.

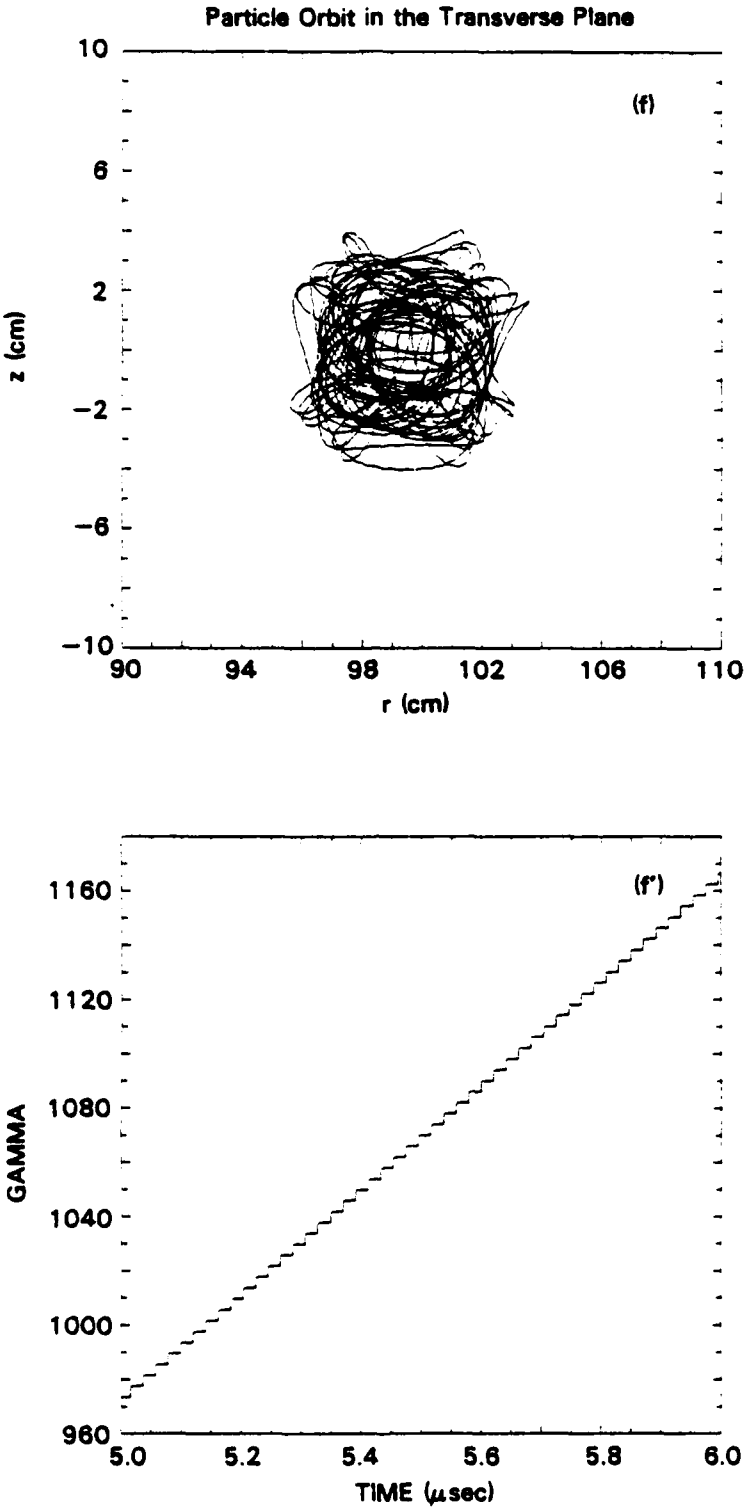

Fig. 10 (Cont'd) — Particle orbit on the (r,z) plane (Figs. 10(a) through 10(j)) and the corresponding relativistic factor γ (Figs. 10(a') through 10(j')). The initial position of the particle is at r = 100 cm, z = 1 cm. The parameters of this run are listed in Table IV.

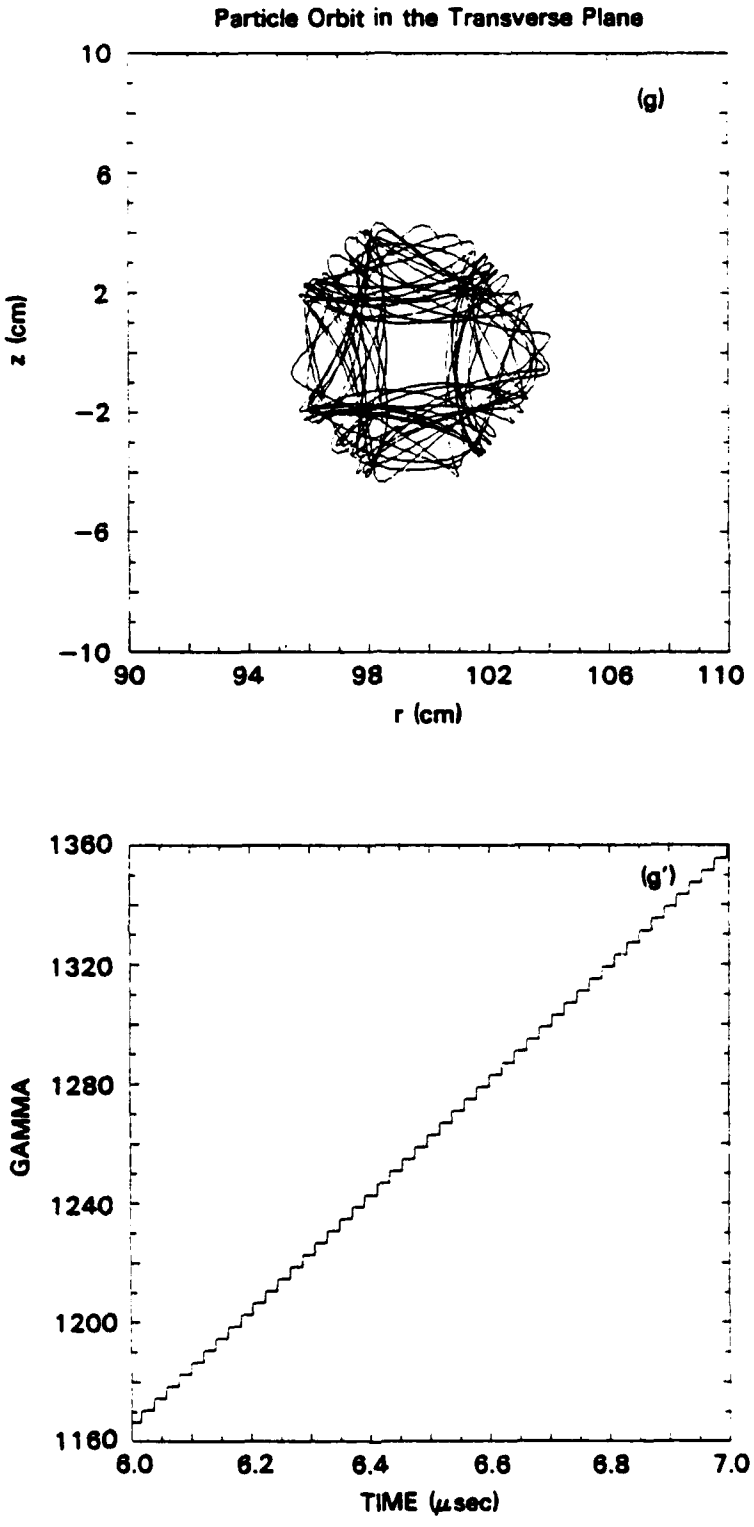

Fig. 10 (Cont'd) — Particle orbit on the (r,z) plane (Figs. 10(a) through 10(j)) and the corresponding relativistic factor γ (Figs. 10(a') through 10(j')). The initial position of the particle is at r = 100 cm, z = 1 cm. The parameters of this run are listed in Table IV.

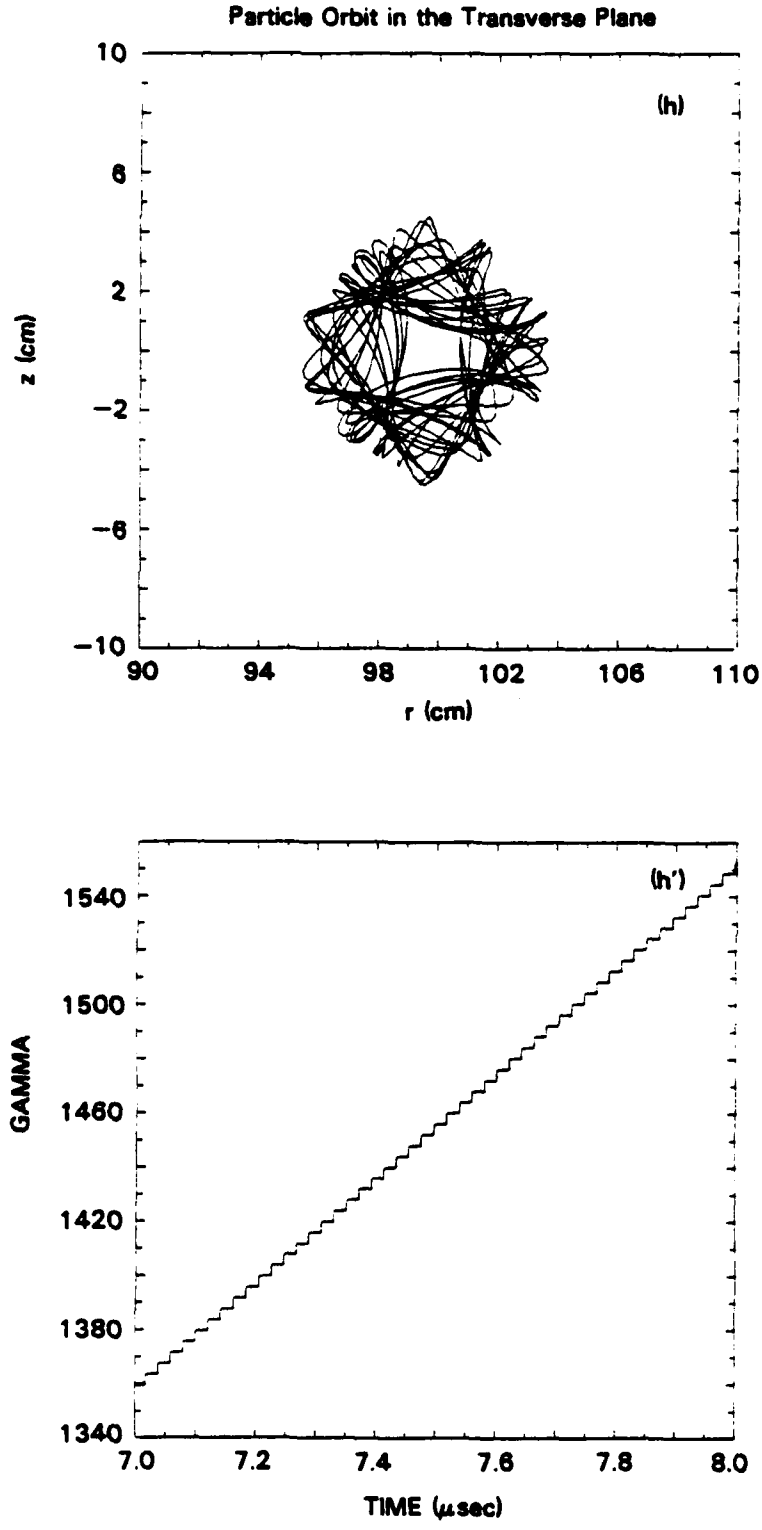

Fig. 10 (Cont'd) — Particle orbit on the (r,z) plane (Figs. 10(a) through 10(j)) and the corresponding relativistic factor γ (Figs. 10(a') through 10(j')). The initial position of the particle is at r = 100 cm, z = 1 cm. The parameters of this run are listed in Table IV.

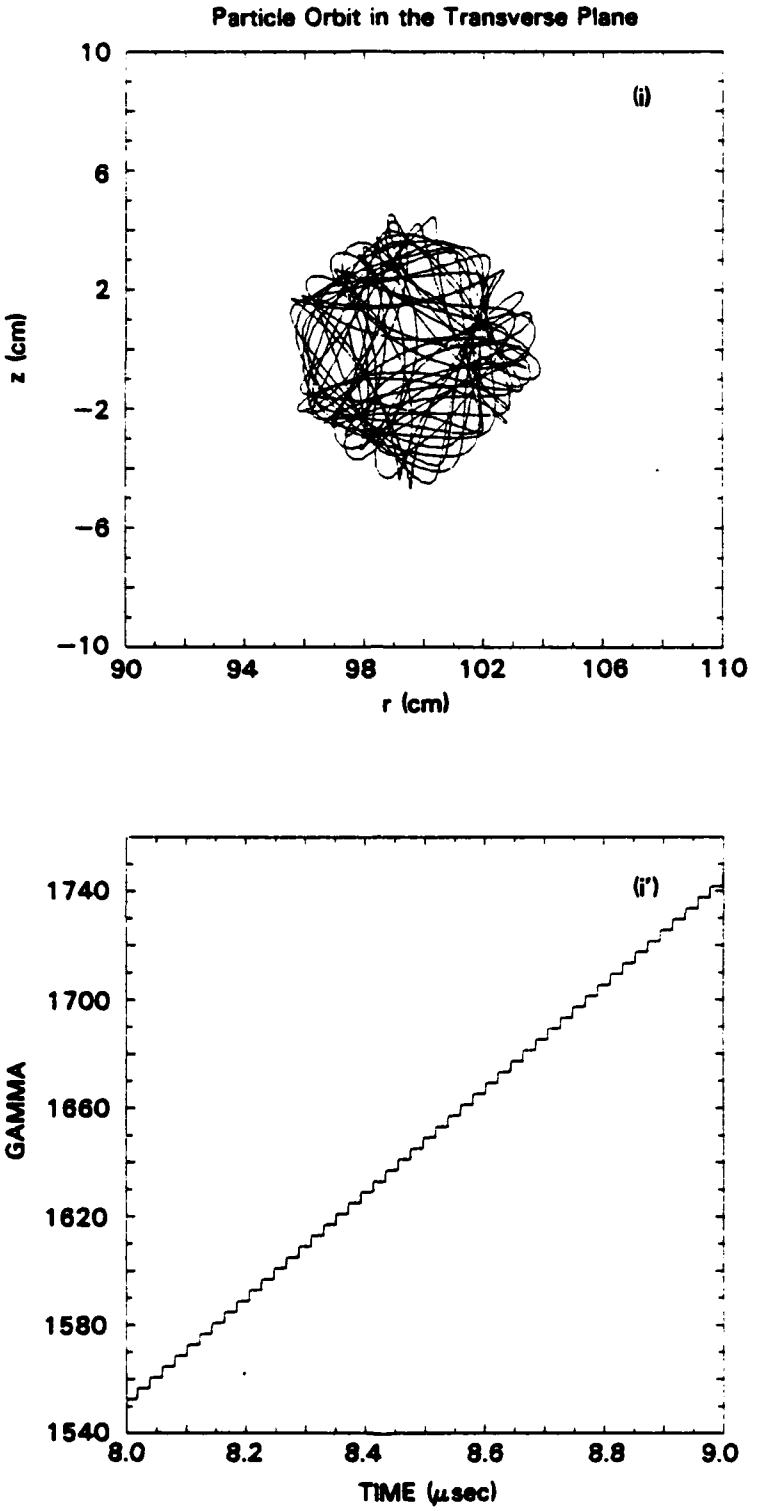

Fig. 10 (Cont'd) — Particle orbit on the (r,z) plane (Figs. 10(a) through 10(j)) and the corresponding relativistic factor γ (Figs. 10(a') through 10(j')). The initial position of the particle is at r = 100 cm, z = 1 cm. The parameters of this run are listed in Table IV.

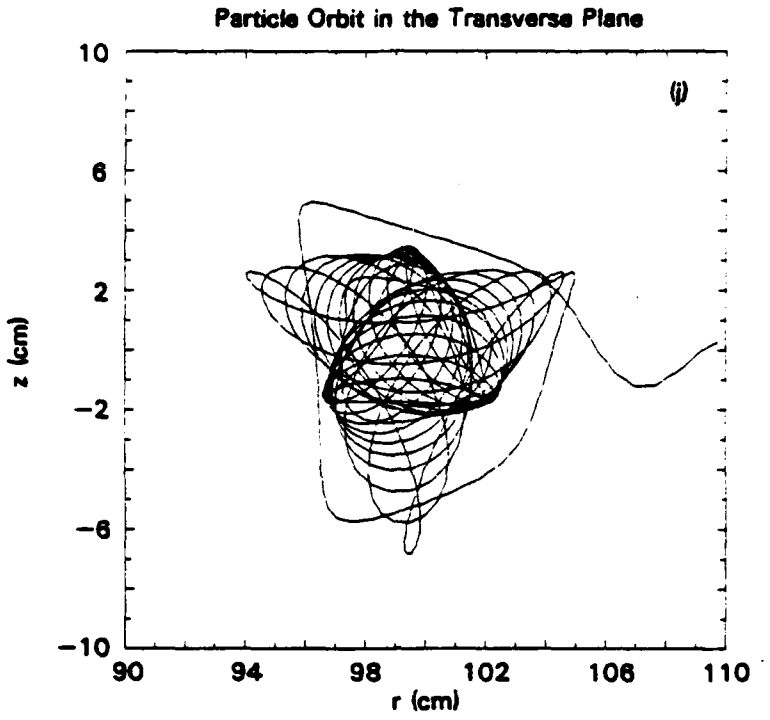

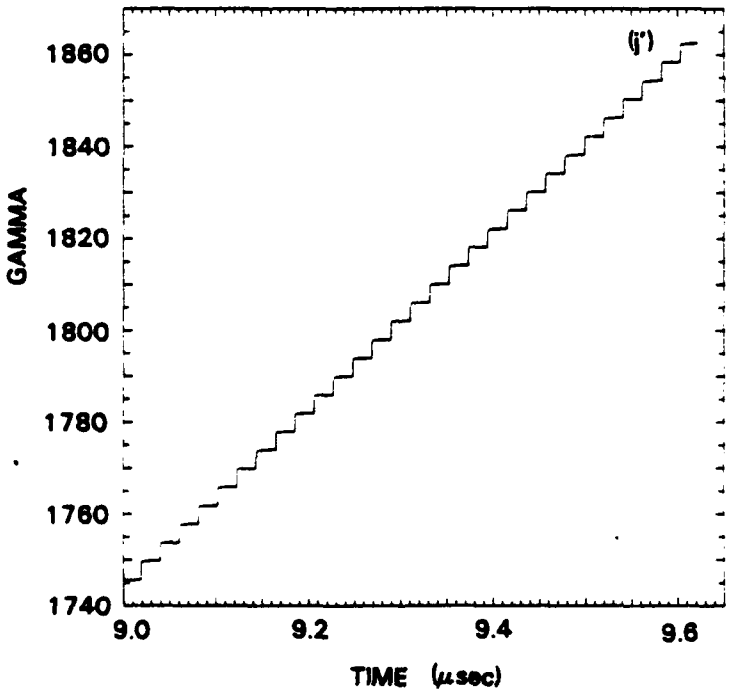

Fig. 10 (Cont'd) — Particle orbit on the (r,z) plane (Figs. 10(a) through 10(j)) and the corresponding relativistic factor γ (Figs. 10(a') through 10(j')). The initial position of the particle is at r = 100 cm, z = 1 cm. The parameters of this run are listed in Table IV.

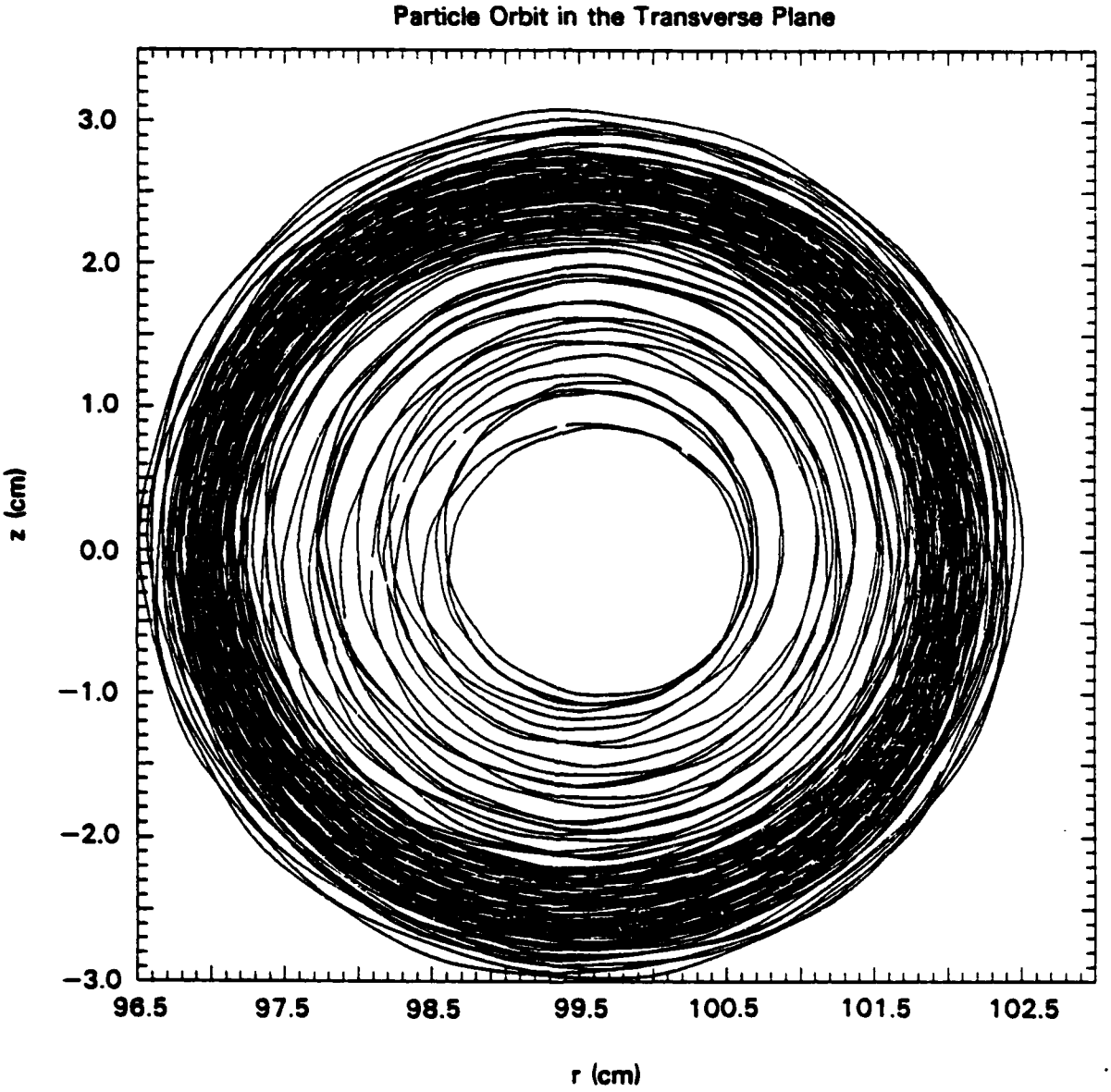

Fig. 11 — This figure is the same as Fig. (9c) on the magnified scale. It demonstrates the expansion of the particle orbit due to the resonance which occurs at $\gamma_z = 522$.

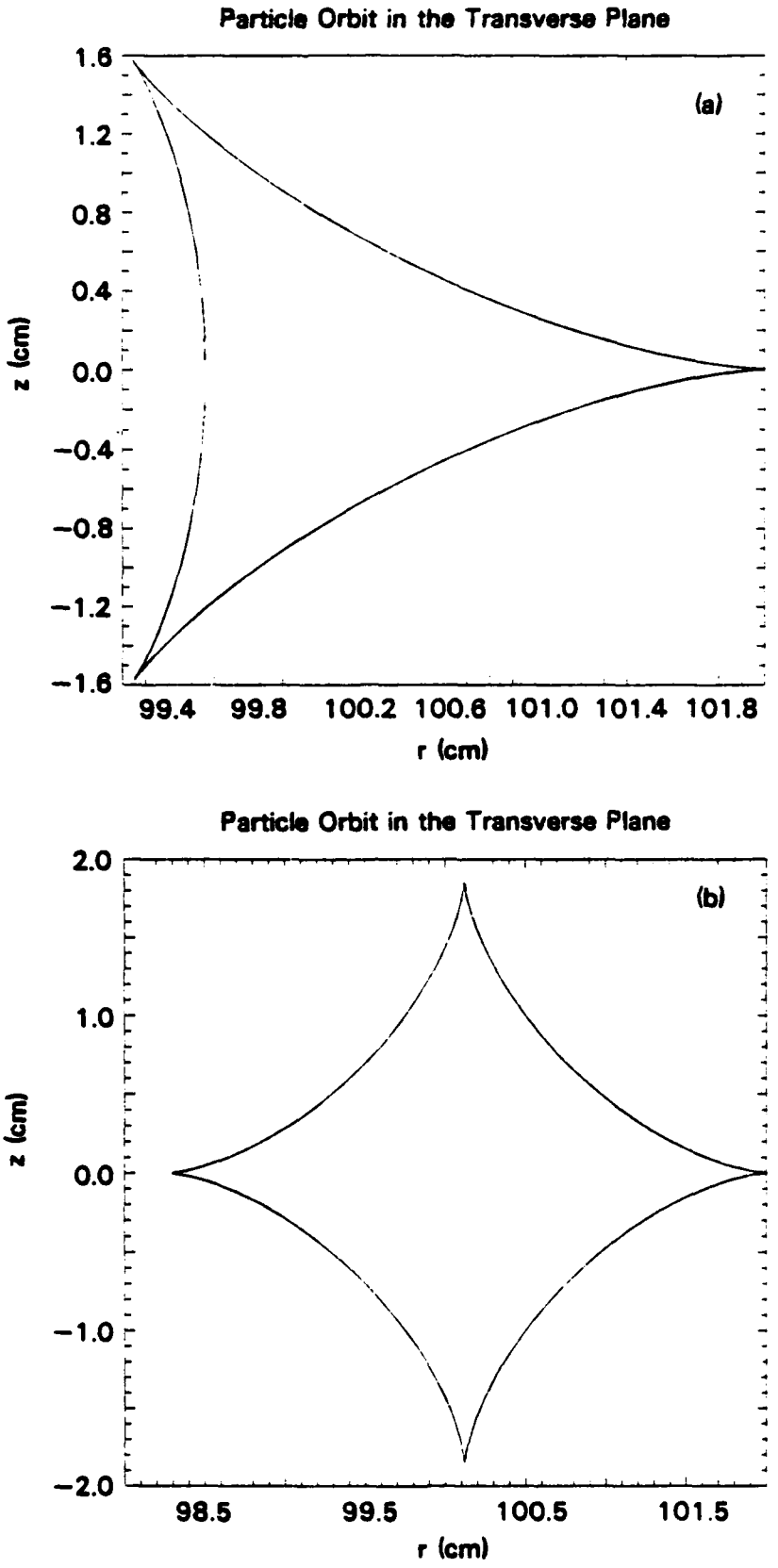

Fig. 12 — Particle orbits without acceleration when the characteristic frequencies of the system become a multiple of each other. This occurs at $\gamma_2 = 1830$ (Fig. 12(a)) and $\gamma_3 = 1121$ (Fig. 12(b)).

Appendix

In the modified betatron, the vector potential is given by the expression[29]

$$A_\theta = B_{zo}\left[\frac{r}{2-n}\left(\frac{r_o}{r}\right)^n + \frac{nz^2}{2r} + \frac{1-n}{2-n}\,\frac{r_o^2}{r}\right], \qquad (A1)$$

where n is the external field index and r_o is the major radius of the torus. Set $r = r_o + x$ and expand Eq. (A1) close to the origin $x = z = 0$. Then, the vector potential is approximately equal to

$$A_\theta \approx B_{zo}\, r_o \left[1 + \frac{1-n}{2}\left(\frac{x}{r_o}\right)^2 + \frac{n}{2}\left(\frac{z}{r_o}\right)^2\right], \qquad (A2)$$

and the rate of change in γ becomes:

$$\gamma = \frac{e}{mc^2}\,\frac{\partial A_\theta}{\partial t}$$

$$= \frac{e}{mc^2} B_{zo}\, r_o \left[1 + \frac{1-n}{2}\left(\frac{x}{r_o}\right)^2 + \frac{n}{2}\left(\frac{z}{r_o}\right)^2\right]. \qquad (A3)$$

The same expression will be shown to be true in the rebatron for the slow motion. Notice that, because of the toroidal structure of the device, the accelerating electric field is periodic with respect to the variable $s_o = -r_o\theta$, with period $2\pi r_o$. Therefore, the E_s component can be Fourier analyzed, i.e.,

$$E_s(x,z,r_o\tilde{\theta}) = A_o(x,z) + \sum_{n=1}^{\infty}\left[A_n(x,z)\cos(n\tilde{\theta}) + B_n(x,z)\sin(n\tilde{\theta})\right]. \qquad (A4)$$

where

$$A_0(x,z) = \frac{1}{2\pi} \int_{-\pi}^{\pi} E_s(x,z,r_0\tilde{\theta})\, d\tilde{\theta} \,, \tag{A5a}$$

$$A_n(x,z) = \frac{1}{\pi} \int_{-\pi}^{\pi} E_s(x,z,r_0\tilde{\theta}) \cos(n\tilde{\theta})\, d\tilde{\theta} \,, \tag{A5b}$$

$$B_n(x,z) = \frac{1}{\pi} \int_{-\pi}^{\pi} E_s(x,z,r_0\tilde{\theta}) \sin(n\tilde{\theta})\, d\tilde{\theta}, \tag{A5c}$$

and $\tilde{\theta} = -\theta$. The position at which the electric field component E_s is computed lies at a fixed distance $r = r_o + x$ from the major axis. Therefore, in order to change the integrals over an angle into line integrals, the transformation $\tilde{\theta} = s/r$ should be made. In particular, under this transformation, Eq. (A5a) becomes:

$$A_0(x,z) = \frac{1}{2\pi r} \int_{-\pi r}^{\pi r} E_s(r,z,s)\, ds. \tag{A6}$$

Since E_s is localized in the region of the accelerating gap, the line integral above is equal to $-V_o$, i.e.,

$$A_0(x,z) = -\frac{V_o}{2\pi r} \,. \tag{A7}$$

The rate of change in γ is approximately equal to

$$\dot{\gamma} = -\frac{e}{mc^2} c \left(-E_s + E_p \right)$$

$$= \frac{e}{mc} \left(E_s + \frac{1}{c} \frac{\partial A_p}{\partial t} \right) . \tag{A8}$$

Replace E_s from Eqs. (A4), (A7) and take into account that $\tilde{\vartheta} \equiv \omega_0 t$, where $2\pi/\omega_0$ is the time period for each revolution around the torus. Then Eq. (A8) can be written as follows:

$$\gamma = \gamma_{slow} + \gamma_{osc} , \tag{A9}$$

where

$$\gamma_{slow} = \frac{e}{mc} \left(- \frac{V_o}{2\pi r} + \frac{1}{c} \frac{\partial A_\theta}{\partial t} \right). \tag{A10a}$$

$$\gamma_{osc} = \frac{e}{mc} \sum_{n=1}^{\infty} \left(A_n(x,z) \cos(n\omega_0 t) - B_n(x,z) \sin(n\omega_0 t) \right). \tag{A10b}$$

The slow motion or the drift of the beam is associated with the first term in Eq. (A9) while the resonances, discussed in Section IIIc, are associated with the second term.

Concentrate on the slow motion and use Eqs. (2.15), (2.19a) and (2.19b). Then Eq. (A10a) becomes:

$$\gamma_{slow} = \frac{e}{mc} \left(- \frac{V_o}{2\pi r} + \frac{I_p}{c^2} \hat{A}_\theta (x,z) \right), \tag{A11}$$

and also

$$\hat{B}_r = - \frac{\partial \hat{A}_\theta}{\partial z} , \tag{A12a}$$

$$\hat{B}_z = \frac{\partial \hat{A}_\theta}{\partial x} + \frac{1}{r} \hat{A}_\theta . \tag{A12b}$$

Take a Taylor expansion of $\hat{A}_\theta(x,z)$ at x=0, z=0, i.e.,

$$\hat{A}_\theta(x,z) \approx \hat{A}_{\theta o} + \frac{\partial \hat{A}_\theta}{\partial x} x + \frac{\partial \hat{A}_\theta}{\partial z} z + \frac{1}{2} \frac{\partial^2 \hat{A}_\theta}{\partial x^2} x^2 + \frac{1}{2} \frac{\partial^2 \hat{A}_\theta}{\partial z^2} z^2 + \frac{\partial^2 \hat{A}_\theta}{\partial x \partial z} xz, \tag{A13}$$

where the partial derivatives are computed at x=0, z=0. It follows from Eqs. (2.23), (2.22a), (2.22b) and (2.18) that

$$\frac{\partial \hat{A}_\theta}{\partial x} = \frac{\partial^2 \hat{A}_\theta}{\partial x \partial z} = 0 \quad . \tag{A14}$$

Also use the identities:

$$\frac{1}{2} \frac{\partial^2 \hat{A}_\theta}{\partial x^2} = \frac{1}{2} \frac{1}{r_o} \hat{B}_{zo} + \frac{1}{2} \frac{\partial \hat{B}_z}{\partial x} - \frac{1}{r_o} \frac{\partial \hat{A}_\theta}{\partial x} \quad , \tag{A15a}$$

$$\frac{1}{2} \frac{\partial^2 \hat{A}_\theta}{\partial z^2} = - \frac{1}{2} \frac{\partial \hat{B}_r}{\partial z} \quad . \tag{A15b}$$

Then Eq. (A11) becomes approximately equal to

$$\gamma_{slow} \approx \frac{e}{mc} \left[- \frac{V_o}{2\pi r_o} + \frac{I_p}{c^2} \hat{A}_{\theta o} + \left(\frac{V_o}{2\pi r_o^2} + \frac{I_p}{c^2} \frac{\partial \hat{A}_\theta}{\partial x} \right) x \right.$$

$$\left. + \left(- \frac{V_o}{2\pi r_o^3} - \frac{I_p}{c^2} \frac{1}{r_o} \frac{\partial \hat{A}_\theta}{\partial x} + \frac{1}{2} \frac{I_p}{c^2} \frac{1}{r_o} \hat{B}_{zo} + \frac{1}{2} \frac{I_p}{c^2} \frac{\partial \hat{B}_z}{\partial x} \right) x^2 - \frac{1}{2} \frac{I_p}{c^2} \frac{\partial B_x}{\partial z} z^2 \right], \tag{A16}$$

where $1/r = 1/(r_o + x)$ was expanded in powers of x. For a matched beam, I_p is given by Eqs. (3.19a), (3.19b) which can also be written as follows (cf. Eq. (A12b)):

$$\frac{1}{c^2} I_p = - \frac{V_o/(2\pi r_o^2)}{\frac{\partial \hat{A}_\theta}{\partial x}} \quad . \tag{A17}$$

Therefore, Eq. (A16) simplifies to the expression

$$\gamma_{slow} = \frac{e}{mc^2} B_{zo} r_o \left[1 + \frac{1}{2}\left(1 + \frac{r_o}{\hat{B}_{zo}} \frac{\partial \hat{B}_z}{\partial x}\right)\left(\frac{x}{r_o}\right)^2 - \frac{1}{2} \frac{r_o}{\hat{B}_{zo}} \frac{\partial \hat{B}_r}{\partial z} \left(\frac{z}{r_o}\right)^2 \approx \right. . \tag{A18}$$

If the linearized expressions for $\hat{B}_r$, $\hat{B}_z$ are used (cf. Eqs. (2.24a), (2.24b)), then Eq. (A18) becomes:

$$\gamma_{slow} = \frac{e}{mc^2} B_{zo} r_o \left[1 + \frac{1 - n_o}{2} \left(\frac{x}{r_o}\right)^2 + \frac{n_o}{2} \left(\frac{z}{r_o}\right)^2 \approx \right. \quad , \tag{A19}$$

which is identical to Eq. (A3) for the modified betatron. Therefore, the rate of change of the mismatch $\delta\gamma$, associated with the slow motion in the rebatron, is a second order effect in the displacement of the beam, that is very small and if the mismatch $\delta\gamma$ is initially zero is will remain negligible. Concequently, the drift of the beam is negligible as observed in the computer runs.

References

*Work is jointly supported by the Office of Naval Research and U.S. Army Ballistic Research Laboratory, Aberdeen, Md.

(a) Permanent Address: Science Applications, Inc., McLean, Va. 22102

(b) Permanent Address: Sachs/Freeman Associates, Bowie, Md. 20715

1. C.A. Kapetanakos and P. Sprangle, Phys. Today, V. 38, #2 (Feb 1985), p. 58.

2. C.A. Kapetanakos and P. Sprangle, NRL Memo Report No. 5259, 1984. **ADA142302**

3. James E. Leiss, IEEE Trans. on Nucl. Sciences NS-26, 3870 (1979).

4. John A. Nation, Particle Accelerators 10, 1 (1979).

5. D. Keefe, Part. Acc. 11, 187 (1981).

6. N.C. Christofilos, et. al., Rev. Sci. Instrum. 35, 886 (1964).

7. J.E. Leiss, N.J. Norris and M.A. Wilson, Part. Acc. 10, 223 (1980).

8. T.J. Fessenden, et. al., Proc. of the Int. Top. Conf. on high power electron and Ion Beam Research and Technology; Palaiseau, France, June 29 - July 3, 1981, p. 813. AD-A057 218, Vol. I, AD A057 219 Vol. II, March 78, edition.

9. R.J. Briggs, et. al., Proc. 1981 Particle Accel. Conf.; IEEE Trans. Nucl. Sci. NS-28 (June 1981), p. 3360.

10. A.I. Pavlovskii, et. al., Sov. Phys. Dokl. 25, 120 (1980).

11. K.R. Prestwich, et. al., IEEE Trans. on Nucl. Sci. NS-30, 3155 (1983).

12. L.N. Kazanskii, A.V. Kisletsov and A.N. Lebedev, Atomic Energy 30, 27 (1971).

13. M. Friedman, Appl. Phys. Lett. 41, 419 (1982).

14. D.W. Kerst, Nature 157, 90 (1946).

15. A.I. Pavlovskii, et. al., Sov. Phys. Tech. Phys. 22, 218 (1977).

16. P. Sprangle and C.A. Kapetanakos, J. Appl. Phys. 49, 1 (1978).

17. N. Rostoker, Comments on Plasma Physics, Vol. 6, p. 91 (1980).

18. C.A. Kapetanakos, P. Sprangle, D.P. Chernin, S.J. Marsh and I. Haber, Phys. Fluids 26, 1634 (1983).

19. C.W. Roberson, A. Mondelli and D. Chernin, Phys. Rev. Lett. 50, 507 (1983).

20. A.A. Mondelli and C.W. Roberson, Particle Accelerators 15, 221 (1984).

21. C.A. Kapetanakos, et. al., NRL memo report no. 5503 (1985); also Part. Accel. 1985. ADA153835

22. L. Teng, Argonne Nat. Lab. Report No. AnLAB-55 (1959); G. Salardi, et. al., Nucl. Instr. and Methodes 59, 152 (1968); R.M. Pearce, Nucl. Instr. and Methodes 83, 101 (1970); R.L. Gluckstern, Proc. Linear Accel. Conf., 1979, p. 245.

23. P. Sprangle and C.A. Kapetanakos, NRL Memo Report No. 5458 (1984); also Part. Accel. (1985). ADA151392

24. C.A. Kapetanakos, D. Dialetis and S.J. Marsh, NRL memo report no. 5619 (1985). ADA161696

25. J.D. Jackson, Classical Electro dynamics (John Wiley & Sons, New York, 1975) p. 178, Eq. (5.37).

26. I.S. Gradshteyn, I.M. Ryzhik, Table of Integrals, Series, and Products (Academic Press, Inc., New York, 1980) pp. 905-906, Eqs. 8.113 and 8.114.

27. D. Chernin and P. Sprangle, Particle Accelerators 12, 101 (1982).

28. H. Knoepfel, Pulsed High Magnetic Fields (North-Holland Publishing Company, Amsterdam, 1970) p. 323, Fig. (A1.21).

29. C.A. Kapetanakos and S.J. Marsh, NRL memo report no. 5387 (1984). ADA148106

END

DTIC

5-86